

AALTO UNIVERSITY SCHOOL OF SCIENCE AND TECHNOLOGY
FACULTY OF ELECTRONICS, COMMUNICATION AND AUTOMATION
DEPARTMENT OF RADIO SCIENCE AND ENGINEERING

Juha-Petri Kärnä

Using statistical inversion for the retrieval of geophysical parameters from remote sensing data

Thesis submitted in partial fulfilment of the requirements for the degree of Licentiate
of Science in Technology.

Espoo, 25th May 2010

Supervisor: Professor Martti Hallikainen

Second examiner: Professor Jouni Pulliainen

ABSTRACT OF LICENTIATE THESIS		AALTO UNIVERSITY SCHOOL OF SCIENCE AND TECHNOLOGY P.O. BOX 11000, FI-00076 AALTO http://www.aalto.fi	
Author Juha-Petri Kärnä			
Name of the thesis Using statistical inversion for the retrieval of the geophysical parameters from remote sensing data			
Date May 25, 2010			
<input type="checkbox"/> Monograph		<input checked="" type="checkbox"/> Article thesis (summary + original articles)	
Faculty	Faculty of Electronics, Communication and Automation		
Department	Department of Radio Science and Engineering		
Professorship	Space Technology, S-92		
Supervisor	Professor Martti Hallikainen		
Second examiner	Professor Jouni Pulliainen		
<p>Abstract</p> <p>In this thesis the use of statistical inversion method for retrieving geophysical parameters from different remote sensing data was studied. The statistical inversion method is rather universal. In this work it was demonstrated by retrieving the following snow and forest parameters: snow depth, snow water equivalent, snow-covered area and forest stem volume.</p> <p>One of the benefits of the statistical inversion method is that it can combine data from different sources based on their statistical accuracy. The method can also estimate the accuracy of the estimation result based on the accuracy of the input data and the models used.</p> <p>In this work the statistical inversion method was demonstrated by retrieving snow depth of Eurasia from microwave radiometer data, snow covered area from microwave and optical data, forest stem volume from ERS INSAR data, and enhancing the accuracy of the discharge forecasts of the operational watershed simulation and forecasting system (WSFS) using SAR data.</p> <p>The statistical inversion method utilises remote sensing models. The Helsinki University of Technology (HUT) microwave snow emission model, the HUT forest backscattering model, and the optical reflectance model developed at the Finnish Environment Institute were used as such. In addition to these remote sensing models, a dynamic environmental model (WSFS) was used to assimilate SAR measurements to it.</p> <p>In addition to the studies mentioned above, two software applications were developed. The first one was developed to simulate brightness temperatures observed by a multichannel microwave radiometer and to test the performance of the available inversion algorithms and the statistical inversion method. The second software application developed is a general purpose statistical inversion tool that can be used either independently or as a part of an image processing system.</p>			
Keywords	Remote sensing, statistical inversion		
URN:	urn:nbn:fi:tkk-013505		
Language	English	Number of pages	95 p. + app. 62 p.
<input checked="" type="checkbox"/> The thesis can be read at http://lib.tkk.fi/Lic/2010/urn013505.pdf			

LISENSIAATINTUTKIMUKSEN TIIVISTELMÄ		AALTO-YLIOPISTO TEKNILLINEN KORKEAKOULU PL 11000, 00076 AALTO http://www.aalto.fi	
Tekijä Juha-Petri Kärnä			
Työn nimi Geofysikaalisten parametrien estimointi kaukokartoitushavainnoista tilastollista inversiota käyttäen			
Päivämäärä 25. toukokuuta 2010			
<input type="checkbox"/> Monografia		<input checked="" type="checkbox"/> Yhdistelmäjulkaisu (yhteenveto + erillisartikkelit)	
Tiedekunta	Elektroniikan, tietoliikennetekniikan ja automaation tiedekunta		
Laitos	Radiotieteen ja -tekniikan laitos		
Professori	Avaruustekniikka, S-92		
Työn valvoja	Prof. Martti Hallikainen		
Toinen tarkastaja	Prof. Jouni Pulliainen		
Tiivistelmä			
<p>Tässä työssä on tutkittu tilastollisen inversion käyttöä geofysikaalisten suureiden estimoinnissa kaukokartoitushavainnoista. Menetelmä on varsin yleispätevä, työssä demonstroitiiin menetelmää metsän runkotilavuuden sekä lumipeitteen ominaisuuksien – paksuuden, vesiarvon ja peittoalan – estimoinnissa.</p> <p>Yksi tilastollisen inversion eduista on eri lähteistä tulevien havaintojen yhdistäminen optimaalisesti, koska menetelmä painottaa eri lähteistä tulevia havaintoja niiden tilastollisen tarkkuuden mukaan. Menetelmä pystyy myös tuottamaan estimoimilleen suureille tarkkuusarvion, joka pohjautuu käytettyjen havaintojen sekä mallien tarkkuuteen.</p> <p>Menetelmää on tässä työssä käytetty koko Euraasian laajuisten lumensyvyyskarttojen luomiseen mikroaaltoradiometrihavainnoista, lumen peittoalan estimoimiseen tutka- ja optisista havainnoista, metsän runkotilavuuden estimoimiseen ERS INSAR-havainnoista sekä operatiivisen vesistömallin (WSFS) virtaamaennusteiden parantamiseen tutkahavaintojen avulla.</p> <p>Menetelmä käyttää hyväkseen kaukokartoitusmalleja. Kaukokartoitusmalleina käytettiin Teknillisessä korkeakoulussa kehitettyä lumen mikroaaltoemissiomallia ja metsän mikroaaltosirontamallia sekä Suomen ympäristökeskuksessa kehitettyä lumen reflektanssimallia. Näiden kaukokartoitusmallien lisäksi käytettiin dynaamista ympäristömallia (WSFS), johon assimiloitiin tutkahavaintoja.</p> <p>Edellämainittujen sovellusten lisäksi työssä kehitettiin myös kaksi ohjelmistoa. Ensimmäinen simuloi monikanavaisen radiometrin havainnoimia kirkkauslämpötiloja testatakseen erilaisia tunnettuja inversioalgoritmeja sekä tilastollista inversiota. Toinen kehitetty ohjelma on yleiskäyttöinen työkalu suureiden estimointiin kaukokartoitushavainnoista tilastollisella inversiolla. Ohjelmaa voi käyttää sellaisenaan tai jonkin kuvankäsittelyjärjestelmän osana.</p>			
Asiasanat	Kaukokartoitus, tilastollinen inversio		
URN:	urn:nbn:fi:tkk-013505		
Kieli	englanti	Sivumäärä	95 s. + liit. 62 s.
<input checked="" type="checkbox"/> Luettavissa verkossa osoitteessa http://lib.tkk.fi/Lis/2010/urn013505.pdf			

Preface

This thesis has been conducted in the former Laboratory of Space Technology of the Helsinki University of Technology (currently a research group in the Department of Radio Science and Engineering of the Aalto University School of Science and Technology).

I would like to express my gratitude to Prof. Martti Hallikainen for acting as the supervisor for my work. I also want to thank my instructor Prof. Jouni Pulliainen, who has given a lot of important ideas to my work and acted as a tutor in all the papers in my thesis.

I also want to thank the whole personnel of the Laboratory of Space Technology for creating a very friendly and inspiring working environment. Especially I am going to remember Skyvan flights with Simo, Kimmo's jokes and sähly coaching, Jaan's spontaneous "Hallelujah" and endless number of ideas, Tuomo's Hissimörkö, Jösse's Helvetinkone, Captain Mustaparta, and Nuijimistalkoot, just to name a few...

During my work I have got help from many colleagues, especially from Panu Lahtinen, Juha Lemmetyinen, Kari Luoju, Matias Takala, and Jarkko "Kossu" Koskinen from Finnish Meteorological Institute and from Sari Metsämäki, Saku Anttila, Markus Huttunen, and Bertel Vehviläinen from Finnish Environment Institute SYKE.

Many thanks to my wife Susanna and to my lovely daughters Peppi and Lotta for their patience during my work. And thanks to my parents, Helvi and Juhani, for their support.

Espoo, May 25th, 2010.

Juha-Petri Kärnä

Contents

Preface	6
Contents	7
List of Publications	9
Author's contribution	10
List of Abbreviations	11
List of Symbols	13
List of Figures	15
List of Tables	17
1 Introduction	18
2 Theoretical background	21
2.1 Modelling of remote sensing observations	21
2.1.1 Linear models	22
2.1.2 Non-linear models	22
2.2 Statistical inversion	23
2.2.1 General method	23
2.2.2 Linear models	24
2.2.3 Nonlinear models	25
2.3 Assimilation of data to dynamic models	25
3 Data	26
3.1 Microwave remote sensing data	26
3.1.1 Microwave radiometer data	26
3.1.2 Radar data	30

3.2	Optical remote sensing data	33
3.3	In situ data	33
3.3.1	Weather station measurements	34
3.3.2	Snow course measurements	34
3.3.3	Auxiliary data	35
4	Models	41
4.1	Linear models	41
4.1.1	Optical reflectance model	42
4.2	Nonlinear models	42
4.2.1	HUT snow emission model	43
4.2.2	HUT forest backscattering model	44
4.3	Dynamic models	48
4.3.1	Watershed Simulation and Forecasting System	49
5	Methodology testing, results and discussion	53
5.1	Statistical inversion method	53
5.2	Statistical inversion with a priori data	59
5.3	Statistical inversion with two data sources	70
5.4	Assimilating data into a dynamic model	75
5.5	A general statistical inversion tool	78
5.6	Software	82
5.6.1	Environment	82
5.6.2	Remote Sensing Software	82
5.6.3	Development Tools	83
5.6.4	Documentation tools	84
6	Conclusions	85
	References	87
	Errata	

List of Publications

This thesis consists of an overview and of the following publications which are referred to in the text by their Roman numerals.

- I** J. Pulliainen, J-P. Kärnä, and M. Hallikainen. 1993. Development of geophysical retrieval algorithms for the MIMR. *IEEE Transactions on Geoscience and Remote Sensing* 31, no. 1, pages 268–277.
- II** J-P. Kärnä, J. Lemmetyinen, M. Hallikainen, P. Lahtinen, J. Pulliainen, and M. Takala. 2007. Operational snow map production for whole Eurasia using microwave radiometer and ground-based observations. In: *Proceedings of the IEEE International Geoscience and Remote Sensing Symposium 2007 (IGARSS'07)*, pages 1456–1459. Barcelona, Spain. 23–28 July 2007.
- III** J-P. Kärnä, J. Pulliainen, K. Luojus, N. Patrikainen, M. Hallikainen, S. Metsämäki, and M. Huttunen. 2004. Mapping of snow covered area using combined SAR and optical data. In: *Proceedings of the 4th International Symposium on Retrieval of Bio- and Geophysical Parameters from SAR Data for Land Applications*. Innsbruck, Austria. 16–19 November 2004.
- IV** J-P. Kärnä, J. Pulliainen, M. Huttunen, and J. Koskinen. 2002. Assimilation of SAR data to operational hydrological runoff and snow melt forecasting model. In: *Proceedings of the IEEE International Geoscience and Remote Sensing Symposium 2002 (IGARSS'02)*, volume 2, pages 1146–1148. Toronto, Canada. 24–28 June 2002.
- V** J-P Kärnä and J. Pulliainen. 2007. A statistical inversion tool for retrieving geophysical parameters from remote sensing data. Report 68, Laboratory of Space Technology, Helsinki University of Technology, Espoo, Finland. ISBN 978-951-22-8636-2, 30 pages.

Author's contribution

In publication I ([P I]) the author was responsible for the design and implementation of the simulation software containing statistical inversion and microwave emission models. The author also run the simulations presented in the paper. Prof. J. Pulliainen managed the whole research project and initiated the paper.

The research work in [P II] was carried out by the author, Mr J. Lemmetyinen providing AMSR-E data processing software, Mr P. Lahtinen providing meteorological data and processing, and Prof. J. Pulliainen acting as a scientific advisor.

The research work in [P III] was carried out by the author, Prof. J. Pulliainen acting as a scientific advisor, Dr. K. Luojus providing RADARSAT data and algorithms, Ms N. Patrikainen and Mrs S. Metsämäki providing AVHRR data, and Mr M. Huttunen assimilating the results into the WSFS hydrological model.

The research work in [P IV] was carried out by the author, Prof. J. Pulliainen acting as a scientific advisor, Mr M. Huttunen helping with the hydrological model, and Prof. J. Koskinen providing SAR data and processing code.

The work in [P V] was carried out by the author, Prof. J. Pulliainen acting as a scientific advisor. The author initiated the publication and implemented the statistical inversion software module.

Prof. M. Hallikainen had the overall responsibility of the projects in which all the work was done as a director of the Laboratory of Space Technology.

List of Abbreviations

AMSR-E	Advanced Microwave Scanning Radiometer for EOS
AVHRR	Advanced Very High Resolution Radiometer
BRDF	Bidirectional Reflectance Distribution Function
CEOS	Committee on Earth Observation Satellites
DEM	Digital Elevation Model
EOS	Earth Observing System
ERS	European Remote Sensing Satellite
ESA	European Space Agency
FMI	Finnish Meteorological Institute
FTP	File Transfer Protocol
GOME	Global Ozone Monitoring Experiment
HDF	Hierarchical Data Format
HH	Horizontal-Horizontal, instrument is transmitting and receiving horizontally polarized radiation
HUT	Helsinki University of Technology
HUTRAD	Helsinki University of Technology radiometer, six-frequency airborne microwave radiometer
HUTSCAT	Helsinki University of Technology scatterometer
IFOV	Instantaneous Field of View
IEEE	Institute of Electrical and Electronics Engineering
INSAR	Interferometric Synthetic Aperture Radar
LAI	Leaf Area Index
MIMR	Multi-Frequency Imaging Microwave Radiometer
MODIS	Moderate Resolution Imaging Spectroradiometer
NASA	National Aeronautics and Space Administration
NSIDC	National Snow and Ice Data Center
NOAA	National Oceanic & Atmospheric Association

RADARSAT	A Canadian remote sensing satellite equipped with a SAR
SAR	Synthetic Aperture Radar
SCA	Snow Covered Area
SMMR	Scanning Multichannel Microwave Radiometer
SSM/I	Special Sensor Microwave Imager
SWE	Snow Water Equivalent
SYKE	Finnish Environment Institute
TKK	Helsinki University of Technology
VV	Vertical-Vertical, see HH
WGS-84	World Geodetic System 1984
WMO	World Meteorological Organization
WSFS	Watershed Simulation and Forecasting System
WWW	World Wide Web

List of Symbols

Γ	Reflectivity
ϵ_n	Measurement error at channel n
θ	Angle of incidence
$\rho(x)$	Probability density distribution
ρ	Optical reflectance
ρ_{forest}	Reflectance of dense forest
ρ_{ground}	Reflectance of snow-free ground
ρ_{snow}	Reflectance of wet snow cover
ρ_{model}	Modelled reflectance
σ	Standard deviation
σ^2	Variance
σ^o	Radar backscattering coefficient
σ_{can}^o	Radar backscattering coefficient of canopy
σ_{ground}^o	Radar backscattering coefficient of ground
σ_{snow}^o	Radar backscattering coefficient of snow covered ground
σ_{model}^o	Modelled backscattering coefficient
Σ	Sum operator
χ	Parameter in HUT scattering model representing vegetation frost status
C	Covariance matrix
d_0	Snow grain size
D	Snow depth
e	Emissivity
f	Remote sensing model
f_{for}	Forest coverage fraction
J	Cost function
N	Number of elements (count) in a set
p	Polarisation (horizontal or vertical)

t	Transmissivity
T_a	Apparent temperature
T_B	Brightness temperature
$T_{B,18H}$	Brightness temperature at 18 GHz horizontal polarization
T_{phys}	Physical temperature
V	Forest stem volume (m ³ /ha)
w	Weighting factor
x_m	Geophysical parameter m
\mathbf{x}	$[x_1, \dots, x_m]^T$
y_n	Remote sensing observation at channel n
\mathbf{y}	$[y_1, \dots, y_n]^T$

List of Figures

3.1	Scanning geometry of the AMSR-E radiometer	29
3.2	AMSR-E brightness temperature images of Finland on 18.7 GHz and 36.5 GHz horizontal channels.	29
3.3	RADARSAT-1 imaging geometry and beam modes.	32
3.4	Weather stations above latitude 55° N providing snow depth data. .	35
3.5	Trace of one snow course in Central Finland.	36
3.6	Number of snow course measurements done on each day in spring 2006, 2007, and 2008.	37
3.7	The locations of snow courses and weather stations in Finland. . . .	38
3.8	Forest stem volume in m ³ /ha of Finland in 0.05° resolution.	40
4.1	HUT snow emission model prediction for emissivity of snow covered terrain and brightness temperatures as a function of SWE.	45
4.2	HUT snow emission model estimation of brightness temperatures of snow covered terrain as a function of snow grain size and as a function of forest stem volume.	46
4.3	Backscattering contributions at 5.4 GHz, HH polarisation, 23° angle of incidence.	48
4.4	Forest canopy transmissivity estimated from HUTSCAT measure- ments for 5.4 GHz channel.	49
4.5	Drainage areas of Finland that the WSFS uses.	50
4.6	Example of river discharge and water level forecast of the WSFS model for river Kemijoki.	52
5.1	Windows of the simulation software showing emission calculation and a subsequent inversion.	57
5.2	Sensitivity of the satellite observed apparent temperature to the snow grain size as a function of snow water equivalent.	59

5.3	The SWE map production process showing input and output files. . .	61
5.4	The flowchart of the SWE inversion method.	63
5.5	Standard deviation of the error of SWE estimate.	64
5.6	Scatter plot of SWE estimates vs. <i>in situ</i> measurements in Russia. .	66
5.7	SWE estimations of Finland on 16th of January, February, March, and April 2008.	67
5.8	Scatter plots of the estimated SWE and SD versus snow course mea- surements for January 16th, February 16th, March 16h, and April 16th 2008.	71
5.9	Snow depth map (in cm) over Eurasia on March 13th, 2007.	71
5.10	Flowchart of the retrieval of SCA from two remote sensing data sets: optical and SAR data.	73
5.11	SCA derived from NOAA AVHRR data, from SAR data, and from both data using statistical inversion.	73
5.12	SCA derived from NOAA AVHRR data of May 5th, 2004 versus SCA from SAR data of May 6th, 2004.	74
5.13	The 14 sub drainage areas near lake Lokka in Northern Finland. . .	77
5.14	Flowchart of the assimilation of remote sensing data into the WSFS model.	77
5.15	Left: Measured discharge, discharge from the model with and without the precipitation correction obtained from the assimilation procedure. Right: Corresponding SCA of the model (spring 1998).	79
5.16	Left: Measured discharge, discharge from the model with and without the temperature correction obtained from the assimilation procedure. Right: Corresponding SCA of the model (spring 2000).	79
5.17	INSAR coherence data set versus forest stem volume data.	80
5.18	Forest stem volume estimations with error bars representing the ac- curacies.	81

List of Tables

3.1	The main characteristics of the AMSR-E instrument.	27
3.2	Resolutions 1–5 of the AMSR-E L2A product.	28
3.3	The main characteristics of the ERS-1 SAR.	30
3.4	Characteristics of the AVHRR channels.	34
5.1	Statistics of snow course measurements on validation days.	65
5.2	Parameters used in the assimilation process.	68
5.3	Validation results of the retrieved snow water equivalent against snow course measurements in spring 2008.	69
5.4	Validation results of the retrieved snow depth against snow course measurements in spring 2008.	69

1 Introduction

Nowadays satellites monitor our planet in many ways. Spaceborne remote sensing has been used for decades to retrieve information of Earth's surface. Various types of remote sensing instruments have been used, most common being imaging optical and microwave instruments. Retrieval of geophysical parameters from satellite data is important in various applications including environment monitoring. Empirical models are most common in interpreting the satellite measurements although some physical models have also been used.

Different instrument types have their own advantages and weaknesses. For example, optical instruments provide information with good resolution (few meters to tens of meters) and easily interpreted content (visible light), but suffer from clouds and darkness.

Microwave instruments on the other hand measure radio frequency signals, that human is not used to interpret. However, they are not dependent on solar illumination nor they suffer from clouds. On the down side they produce somewhat lower resolution images, especially passive microwave instruments that typically have a footprint of kilometers or even tens of kilometers.

If good spatial resolution and spatially and timely extensive coverage is needed, the only possibility is to use a combination of optical and microwave instruments. This is possible to do and has been done. Difficulties arise from the differences of the instruments: different resolution, time of acquisition and physical phenomena behind the measured signal.

From the mathematical point of view the statistical inversion promises to combine different data optimally [16]. The method searches the inverse solution of the re-

remote sensing model representing the actual measurement. It takes into account the different accuracies of the data, weighting the data accordingly, finding the solution having the maximum likelihood.

Many *in situ* measurements are done in the Earth's surface, one of the biggest being the world wide weather station network. From the point of view of remote sensing *in situ* measurements are usually used to validate the results obtained by remote sensing methods. But these measurements can also be combined with remote sensing observations to enhance retrieval accuracy.

Literally numerous retrieval algorithms have been developed during the last decades for different remote sensing sensors for different applications. The most common type of algorithms seems to be empirically determined linear algorithms that have been obtained by fitting remote sensing observations to the reference data using linear regression. But when the knowledge of the underlying physics increases, more and more accurate physical models are developed.

Statistical inversion methods have been used in some extent to remote sensing applications. In the atmospheric applications statistical inversion has been used to retrieve atmospheric parameters like temperature and water vapour profiles using radiative transfer model and radiosondes [14] and atmospheric structure constant and wind velocity [13]. In the land applications, statistical inversion has been used to retrieve the soil moisture from radar measurements [9],[50], surface albedo from BRDF measurements [41], and vegetation leaf area index (LAI) from reflectance measurements [8]. Snow water equivalent retrieval using microwave radiometer data with hydrological snow models has been reported in [67]. Pulliainen [43] and Pardé et al. [40] have performed snow water equivalent estimation using statistical inversion with the HUT snow emission model [46]. The statistical inversion method has also been used in the water quality mapping from AVHRR data [64], and from the optical spectroradiometer observations together with *in situ* measurements [45].

This work concentrates on the geophysical parameter retrieval from remote sensing data using statistical inversion methods. While the retrieval method is universal, most of the work presented concerns with the retrieval of snow parameters like snow covered area (SCA) and snow water equivalent (SWE). Various types of remote sensing data have been used: data from optical instruments and from both active and passive microwave instruments. Also the previously mentioned weather station data have been used together with the remote sensing data to improve the snow water equivalent retrieval accuracy.

The statistical inversion method was also used to assimilate remote sensing observations to a dynamic model. The model was the hydrological watershed simulation and forecasting system (WSFS) of the Finnish Environment Institute. By assimilating SAR observations to the model, the internal state variable (snow covered area) were affected towards the right direction, thereby enhancing the forecasting accuracy of the model.

In the following chapters the background information needed to understand the work presented in papers is described. Chapter 2 introduces some theory: modelling of remote sensing observations and the statistical inversion method. Chapter 3 familiarises the reader with the remote sensing data used in the work. Chapter 4 introduces the remote sensing models used in the work and the WSFS hydrological model. Chapter 5 presents the statistical inversion methods used in this work and the results achieved. Finally, Chapter 6 concludes the presented work.

2 Theoretical background

This section introduces the theoretical background of modelling remote sensing observations and the statistical inversion method.

2.1 Modelling of remote sensing observations

Since modelling of remote sensing observations is an important part of the assimilation process, it is discussed first. The relevant equations are introduced here. They are described in more detail in [42] and in mathematical form in [23], which is based on [58] and [59].

Multi-channel remote sensing observations can be described as a function of geophysical parameters using modelling:

$$\mathbf{y} = \mathbf{f}(\mathbf{x}) + \boldsymbol{\epsilon}, \quad (2.1)$$

where $\mathbf{y} = [y_1, \dots, y_n]^T$, $\mathbf{x} = [x_1, \dots, x_m]^T$, $\boldsymbol{\epsilon} = [\epsilon_1, \dots, \epsilon_n]^T$ and \mathbf{f} is the remote sensing model (also called *forward model*) describing multi-channel remote sensing observations.

Parameter y_n is the remote sensing observation at channel n , x_m is the value of the geophysical parameter m at the observation moment, and ϵ_n is the random measurement error at channel n including instrument measurement accuracy and geophysical noise due to non-ideality of the remote sensing model \mathbf{f} .

In the general case, the function \mathbf{f} is non-linear, but when it is linear, the mathematics become much simpler. Therefore the two cases, linear and non-linear, are discussed separately in the following.

2.1.1 Linear models

A linear model describes the remote sensing measurement y at channel i as a function of variable \mathbf{x} :

$$y_i = \beta_{i1}x + \beta_{i2} + \epsilon_i = f_i(\mathbf{x}) + \epsilon_i, \quad (2.2)$$

where ϵ_i is the random error of the model at channel i , β_{i1} and β_{i2} denote the (usually empirical) model parameters.

The model parameters can be estimated fitting the model to a learning data set for each channel separately [42]:

$$\begin{cases} b_{i1} &= \hat{\beta}_{i1} = \frac{N \sum_{k=1}^N x_k y_{ik} - \sum_{k=1}^N x_k \sum_{k=1}^N y_{ik}}{N \sum_{k=1}^N x_k^2 - (\sum_{k=1}^N x_k)^2} \\ b_{i2} &= \hat{\beta}_{i2} = \bar{y}_i - \bar{b}_{i1} \bar{x} \end{cases} \quad (2.3)$$

where x_k is the variable k of the learning data set, and y_{ik} describes the corresponding remote sensing observation. N is the total number of elements in the learning data set.

2.1.2 Non-linear models

Non-linear models are quite common models in describing real world phenomena. They exist in many various forms, one common type being the radiative transfer model [4]. It is used commonly in remote sensing applications, for example for describing the effect of the atmosphere. It has the form of

$$y = ae^{2cx} + b(1 - e^{2cx}), \quad (2.4)$$

with three scalar parameters: a , b , and c .

2.2 Statistical inversion

2.2.1 General method

Using statistical inversion to retrieve geophysical parameters is based on the assumption that the measurements \mathbf{y} , measurement errors $\boldsymbol{\epsilon}$ and geophysical variables \mathbf{x} are random variables that are characterised by their probability distributions. According to the Bayes theorem [2] it is possible to write a conditional probability equation for the geophysical parameters \mathbf{x} given the remote sensing observations \mathbf{y} . Assuming the modelling errors having a Gaussian distribution, we can write the conditional probability density distribution [16]

$$\rho(\mathbf{y}|\mathbf{x}) = \frac{1}{(2\pi)^{n/2}|\mathbf{C}|^{1/2}} \exp\left(-\frac{1}{2}(\mathbf{y} - \mathbf{f}(\mathbf{x}))^T \mathbf{C}^{-1}(\mathbf{y} - \mathbf{f}(\mathbf{x}))\right), \quad (2.5)$$

where \mathbf{C} is the covariance matrix of the modelling errors between different channels, $\mathbf{y} = [y_1, \dots, y_n]^T$ and \mathbf{f} denotes remote sensing model(s) that describe the observations \mathbf{y} as a function of \mathbf{x} .

If the modelling errors between channels are independent, the covariance matrix \mathbf{C} becomes a diagonal matrix. Then we get a so called cost function $J(\mathbf{x})$ from the exponent part of (2.5) where the minimum of $J(\mathbf{x})$ gives the values of \mathbf{x} which maximise the probability equation. The $J(\mathbf{x})$ is then

$$J(\mathbf{x}) = \sum_{i=1}^n \frac{1}{2\sigma_i^2} (y_i - f_i(\mathbf{x}))^2, \quad (2.6)$$

where σ_i is the standard deviation of the modelling error at channel i .

When additional information of the statistical properties of geophysical parameters exist, we get according to Bayes theorem in case of one estimated parameter x with a known average \hat{x}_{REF} and standard deviation σ_{REF} :

$$\rho(x|\mathbf{y}) = \frac{\rho(\mathbf{y}|x)\rho(x)}{\rho(\mathbf{y})} = \frac{\rho(\mathbf{y}|x)\rho(x)}{1} = \rho(\mathbf{y}|x)\rho(x), \quad (2.7)$$

where $\rho(\mathbf{y}|x)$ is the same as (2.5) and

$$\rho(x) = \frac{1}{(2\pi)^{1/2}\sigma_{REF}} \exp\left(-\frac{1}{2}\left(\frac{\hat{x}_{REF} - x}{\sigma_{REF}}\right)^2\right). \quad (2.8)$$

Using (2.5), (2.7), and (2.8) we get a cost function for the case of one geophysical parameter x :

$$J(x) = \sum_{i=1}^n \frac{1}{2\sigma_i^2} (y_i - f_i(x))^2 + \frac{1}{2\sigma_{REF}^2} (\hat{x}_{REF} - x)^2, \quad (2.9)$$

which differs from the (2.6) only by the last term.

For the case of m geophysical parameters we get:

$$J(x) = \sum_{i=1}^n \frac{1}{2\sigma_i^2} (y_i - f_i(x))^2 + \sum_{j=1}^m \frac{1}{2\sigma_{REF,j}^2} (\hat{x}_{REF,j} - x_j)^2. \quad (2.10)$$

2.2.2 Linear models

Assuming the modelling errors at different channels are normally distributed with the bias of zero having a standard deviation of σ_i we can write an equation for the best estimate for the unknown x :

$$\hat{x} = \frac{\sum_{i=1}^n \frac{1}{\sigma_i^2} b_{i1} (y_i - b_{i2}) + \frac{1}{\sigma_{REF}^2} \hat{x}_{REF}}{\sum_{i=1}^n \frac{1}{\sigma_i^2} b_{i1}^2 + \frac{1}{\sigma_{REF}^2}}. \quad (2.11)$$

For the variance of the estimate \hat{x} we can write [42, p. 81]:

$$var(\hat{x}) = \frac{\sum_{i=1}^n \left(\frac{1}{\sigma_i} b_{i1}\right)^2 + \frac{1}{\sigma_{REF}^2}}{\left(\sum_{i=1}^n \frac{1}{\sigma_i^2} b_{i1}^2 + \frac{1}{\sigma_{REF}^2}\right)^2}. \quad (2.12)$$

2.2.3 Nonlinear models

In the general case the the functions $f_i(x)$ are not linear, and the solution is the global minimum of the cost function (2.6), which gives the maximum *a posteriori* probability to x , which can be searched by iteration.

The variance of the estimate \hat{x} can be formulated as [42, p. 91]

$$var(\hat{x}) = \frac{\sum_{i=1}^n \left(\frac{J_i}{\sigma_i}\right)^2}{\left(\sum_{i=1}^n \left(\frac{J_i^2}{\sigma_i^2}\right) + \frac{1}{\sigma_{REF}^2}\right)^2} + \frac{\frac{1}{\sigma_{REF}^2}}{\left(\sum_{i=1}^n \left(\frac{J_i^2}{\sigma_i^2}\right) + \frac{1}{\sigma_{REF}^2}\right)^2}, \quad (2.13)$$

where

$$J_i = \frac{\partial f_i(x)}{\partial x}.$$

2.3 Assimilation of data to dynamic models

When a dynamic model, for example an environment model, is used in the statistical inversion process, the process is usually called data assimilation instead of statistical inversion. The goal is then to guide or tune the dynamic model to the right direction by the assimilated measurement data instead of estimating a particular geophysical parameter. The process is usually continuous, the measurement data is assimilated to the dynamic model continuously.

The same cost function presented earlier in this chapter still applies in this case although it is more complex since the model parameters are typically changed backwards in time.

An example of the assimilation of remote sensing data is presented in [P IV] where SCA retrieved from SAR data was fed into a hydrological model.

3 Data

In this section the remote sensing data and *in situ* measurements relevant to this work are introduced.

Remote sensing instruments are usually divided into two categories based on the wavelength they measure: optical instruments and microwave instruments. The microwave instruments are still divided into passive and active instruments. This categorisation is used in this section.

3.1 Microwave remote sensing data

Microwave instruments operate at microwave range of electromagnetic spectrum. They can be divided into two main classes: active and passive instruments. Active instruments send signals and receive the reflected signal. Typical active instruments are radars and scatterometers. Passive instruments, called radiometers, do not send anything, they just measure thermal electromagnetic radiation from the target.

3.1.1 Microwave radiometer data

Microwave radiometers are remote sensing instruments that measure thermal radiation at certain radio frequency bands, usually around 1 GHz to 100 GHz. They measure brightness temperature, usually marked as T_B , which is [60, p. 201]

$$T_B = e \cdot T_{phys}, \quad (3.1)$$

where e is the emissivity of the target and T_{phys} is the physical temperature of the target. Emissivity e is defined as $1 - \Gamma$, where Γ is the reflectivity of the target

Table 3.1: The main characteristics of the AMSR-E instrument.[18]

Center frequency (GHz)	6.925	10.65	18.7	23.8	36.5	89.0
Bandwidth (MHz)	350	100	200	400	1000	3000
Polarisation	H and V					
Sensitivity (K)	0.3	0.6	0.6	0.6	0.6	1.1
IFOV cross× along track (km)	43×75	29×51	16×27	18×32	8.2×14	3.7×6.5
Swath width (km)	1450					
Incidence angle (degrees)	55					

which is dependent on the dielectric properties of the target according to Fresnell equations. Surface characteristics, like surface roughness, also affect the emissivity [5].

Microwave radiometers have been flown in satellites since 1970's including SMMR which was launched in 1978 [36]. Typically spaceborne radiometer instruments are equipped with a scanning mechanism to generate an image of the individual measurements (see Figure 3.1).

AMSR-E

One of the latest spaceborne microwave radiometer is the AMSR-E (Advanced Microwave Scanning Radiometer for EOS) [18]. It is a twelve-channel, six-frequency microwave radiometer mounted on the polar orbiting EOS-Aqua satellite. It measures brightness temperatures at six frequencies, from 6.9 GHz to 89 GHz, each in both polarisations, horizontal and vertical, with an incident angle of 55 degrees (see table 3.1).

Table 3.2: Resolutions 1–5 of the AMSR-E L2A product.[30] S means smoothed data and X non-smoothed data.

Resolution no	Footprint size (km×km)	Channel					
		6.9	10.65	18.7	23.8	36.5	89.0
1	75×43	S & X	S	S	S	S	S
2	51×29		S & X	S	S	S	S
3	27×16			X	S & X	S	S
4	14×8					X	S
5	6×4						X

The AMSR-E data are available free of charge from NSIDC (National Snow and Ice Data Center) via FTP and WWW. The data are available on several formats from raw data to ready products. The so called level 2A data product is a radiometrically corrected product needing geometric rectification [15].

Since AMSR-E measurements of different frequencies do not describe identical locations, low level processing with the Level 2A (L2A) algorithm produces spatially consistent data sets, referred to as resolution 1 through 5 as listed in Table 3.2. For this purpose, the L2A algorithm linearly combines brightness temperatures from the Level 1 processing. The L2A data are delivered in HDF-EOS format [55], which is an extension to the hierarchical data format (HDF).

The rectification and mosaicing of data was done in this work in [P II] using a program developed in TKK by Mr. Juha Lemmetyinen [24]. An alternative to that is NASA’s recently released HDF-EOS To GeoTIFF Conversion tool (HEGtool), which allows users to reformat, re-project, stitch/mosaic and subset HDF-EOS images [34].

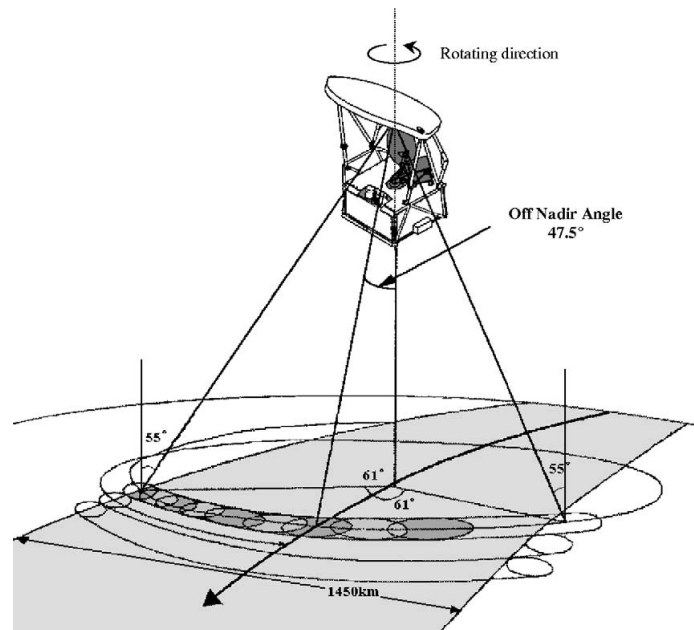


Figure 3.1: Scanning geometry of the AMSR-E radiometer [18].

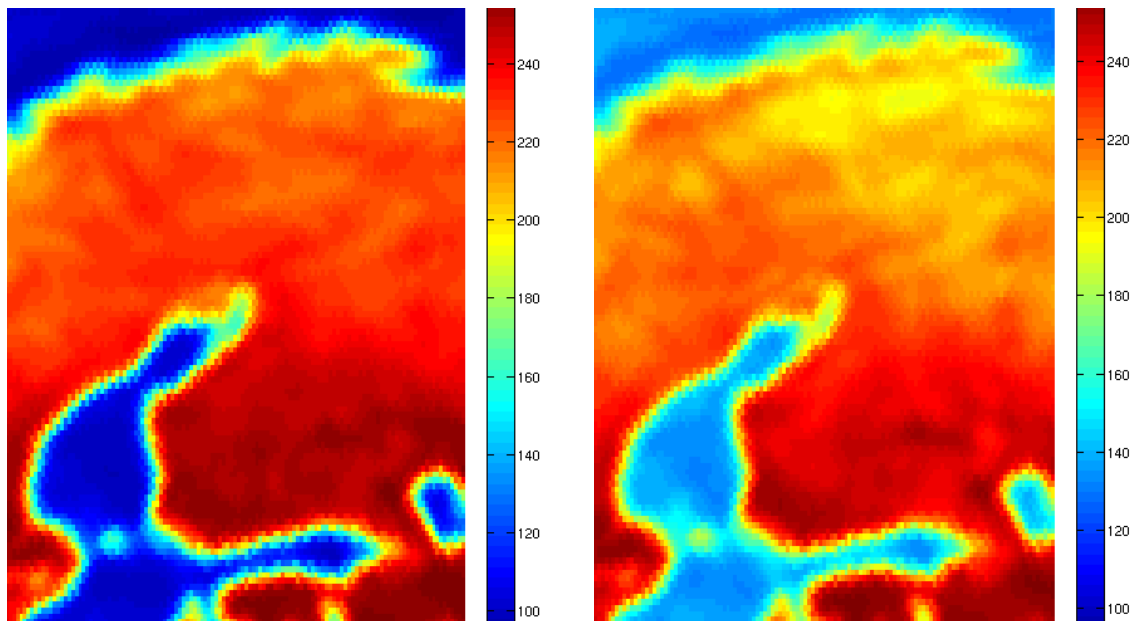


Figure 3.2: AMSR-E brightness temperature images of Finland on 18.7 GHz (left) and 36.5 GHz (right) horizontal channels. Two swaths are combined and rectified to 0.125 degree resolution. Data were acquired on March 18th, 2008 at $01:00$ and $02:39$ UTC.

Table 3.3: The main characteristics of the ERS-1 SAR.

Sensor	Active microwave instrument
Frequency	5.3 GHz (C-band)
Wavelength	5.66 cm
Polarisation	VV
Incident angle	19–28 deg (23 deg mid-swath)
Spatial resolution	22 m × 26 m

3.1.2 Radar data

Microwave radars used in satellites are nowadays mainly synthetic aperture radars (SAR). Using synthetic aperture the antenna does not need to be huge in size in order to have good ground resolution. Instead, the good ground resolution is achieved using clever processing of the sent and received signal [38].

ERS

The first European Remote Sensing satellite, ERS-1, was launched on 17 July 1991 into a near-polar orbit. The ERS-1 includes a C-band (5.3 GHz) synthetic aperture radar (SAR). The main parameters of the ERS-1 SAR are shown in Table 3.3. ERS-1 data are available from 30 July 1991 to 10 March 2000.[61]

ERS-2, the successor of ERS-1, was launched on 21 April 1995. Together, the ERS satellites are now orbiting in the same orbital plane, with all instruments simultaneously operating. ERS-2 is similar to ERS-1 with very similar instruments, only the GOME (Global Ozone Monitoring Experiment) instrument has been added. ERS-2 data are available from 13 July 1995 to current day (except from 17 January

2001 to Autumn 2001 due to gyro failure).

The ERS-1/2 Tandem mission was conducted in 1995–96 while both satellites were in the same orbital plane. ERS-2 imaged the same area on ground 24h after ERS-1. These collected image pairs have been used in interferometric studies, therefore they are known as INSAR data [44].

Available data products of ERS-1/2 include:

- SAR Precision Image Product (PRI)
- SAR Single Look Complex Image Product (SLC)
- SAR Annotated Raw Data Product (RAW)
- SAR Ellipsoid Geocoded Image Product (GEC)
- SAR Wave Mode Fast Delivery Product (SWM)

All the image products cover approximately a $100 \text{ km} \times 100 \text{ km}$ area.

ERS-2 Precision Image Products (PRI) were used in [P IV] and INSAR images (SLC) in [P V].

RADARSAT

RADARSAT is a Canadian remote sensing satellite that carries a Synthetic Aperture Radar (SAR) as its main instrument. The radar operates at C-band at 5.3 GHz using horizontal polarisation for transmitting and receiving (HH-polarisation) [49]. Several image types are available depending on the beam mode used as depicted in Fig. 3.3.

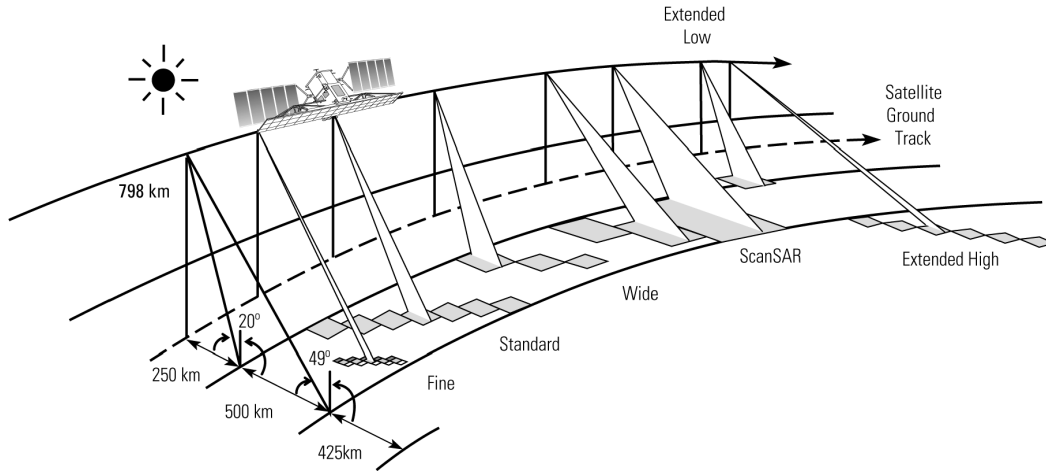


Figure 3.3: RADARSAT-1 imaging geometry and beam modes [49].

The RADARSAT images are path oriented and they are distributed in CEOS (Committee on Earth Observation Satellites) format [6]. RADARSAT images covering Finland are received and processed at Kongsberg Satellite Services (KSAT) in Tromsø, Norway.

ScanSAR Wide images have been used in this work, in [P III]. They cover a $500 \text{ km} \times 500 \text{ km}$ area with a 50 m pixel size having a 100 m spatial resolution. Since the image area is so large, the incident angle varies inside the image typically from 20 degrees to 45 degrees. ScanSAR images can have either 8- or 16-bit values for each pixel.

Since the ScanSAR images are path oriented they have to be rectified to a geographical coordination. The author has developed a rectification program for this purpose [17].

3.2 Optical remote sensing data

Optical imaging instruments have been flown in satellites since late 1960's. They are usually multi-channel instruments, most of channels recording visible light, and a couple of channels recording infrared radiation.

NOAA AVHRR

NOAA Advanced Very High Resolution Radiometer (AVHRR) is a series of spaceborne imaging instruments. The first AVHRR was a 4-channel imaging radiometer, first carried on TIROS-N (launched October 1978). This was subsequently improved to a 5-channel instrument (AVHRR/2) that was initially carried on NOAA-7 (launched June 1981). The latest instrument version is AVHRR/3, with 6 channels, first carried on NOAA-15 launched in May 1998.

The AVHRR/3 has three solar channels in the visible-near infrared region and three thermal infrared channels [35]. The resolution is 1.1 kilometers at nadir. Table 3.4 lists the most important characteristics of the six channels. The AVHRR channel 1 data were used in [P III] to retrieve the snow covered area (SCA).

3.3 In situ data

In addition to remote sensing data some *in situ* measurement data sets have been used in this work. The meteorological data described in the following chapter have been used together with the remote sensing data, while the snow course measurements have been used as reference data in validation.

Table 3.4: Characteristics of the AVHRR channels.[35]

Channel number	Resolution	Wavelength μm	Typical use
	at nadir (km)		
1	1.09	0.58–0.68	Daytime cloud and surface mapping
2	1.09	0.725–1.00	Land-water boundaries
3A	1.09	1.58–1.64	Snow and ice detection
3B	1.09	3.55–3.93	Night cloud mapping, sea surface temperature
4	1.09	10.30–11.30	Night cloud mapping, sea surface temperature
5	1.09	11.50–12.50	Sea surface temperature

3.3.1 Weather station measurements

The synoptic weather station network of World Meteorological Organization (WMO) constitute one of the largest measurement network in the world. The synoptic stations measure continuously several physical parameters like temperature, wind speed, rain and snow depth. Figure 3.4 shows the weather stations providing snow depth data. Snow depth measurements from weather stations were used in [P II]. The data were received from the Finnish Meteorological Institute.

3.3.2 Snow course measurements

Snow course is a measurement line of few kilometers (typically 4 km) on land, which contains different types of terrain (pine, spruce, and birch dominated forest, mixed forest, bog, open area) [53], see Figure 3.5 for an example.

The depth of snow is measured at every 50 meters, typically from about 80 points,

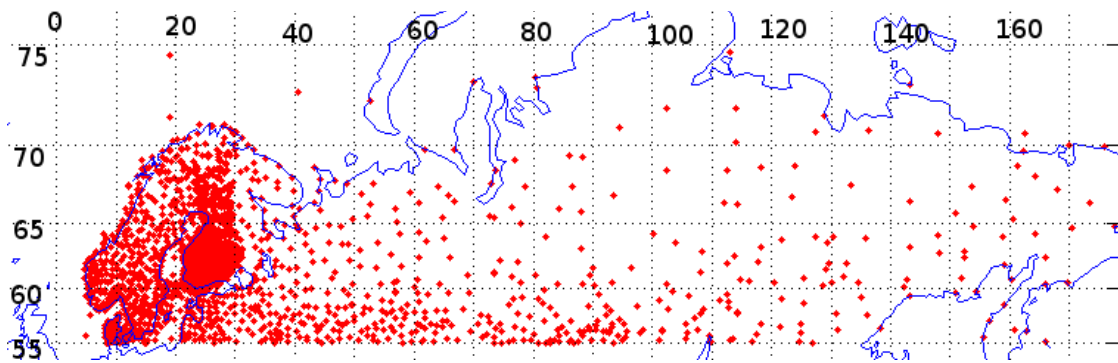


Figure 3.4: Weather stations above latitude 55° N providing snow depth data on February 2008.

while the snow density is measured typically from 8 points [37].

The measurements are done in winter months (November to May) usually at 1st and 16th day of the month (see Figure 3.6 for illustration of measurement activity). Currently there are around 100 active snow courses (93 was measured in spring 2008). Snow course measurements are done by SYKE. Figure 3.7 shows the areal distribution of the snow courses. These measurements provide excellent validation data for snow depth estimations. Snow depth maps of [P II] are validated against these measurements.

3.3.3 Auxiliary data

In addition to remote sensing and *in situ* measurements, some auxiliary data sets have been used. These are for example forest stem volume map of Finland, digital elevation model (DEM), water masks, and drainage area map.

A forest stem volume map from National Board of Survey provided the stem volume needed to classify SAR data into six different classes based on the forest stem volume in [P III] and in [P IV]. Also the HUT backscattering model and HUT snow emission



Figure 3.5: Trace of one snow course in Central Finland shown in white line. The white grid represents 1 km by 1 km area. Forested areas show in dark and open areas in light colors.[32]

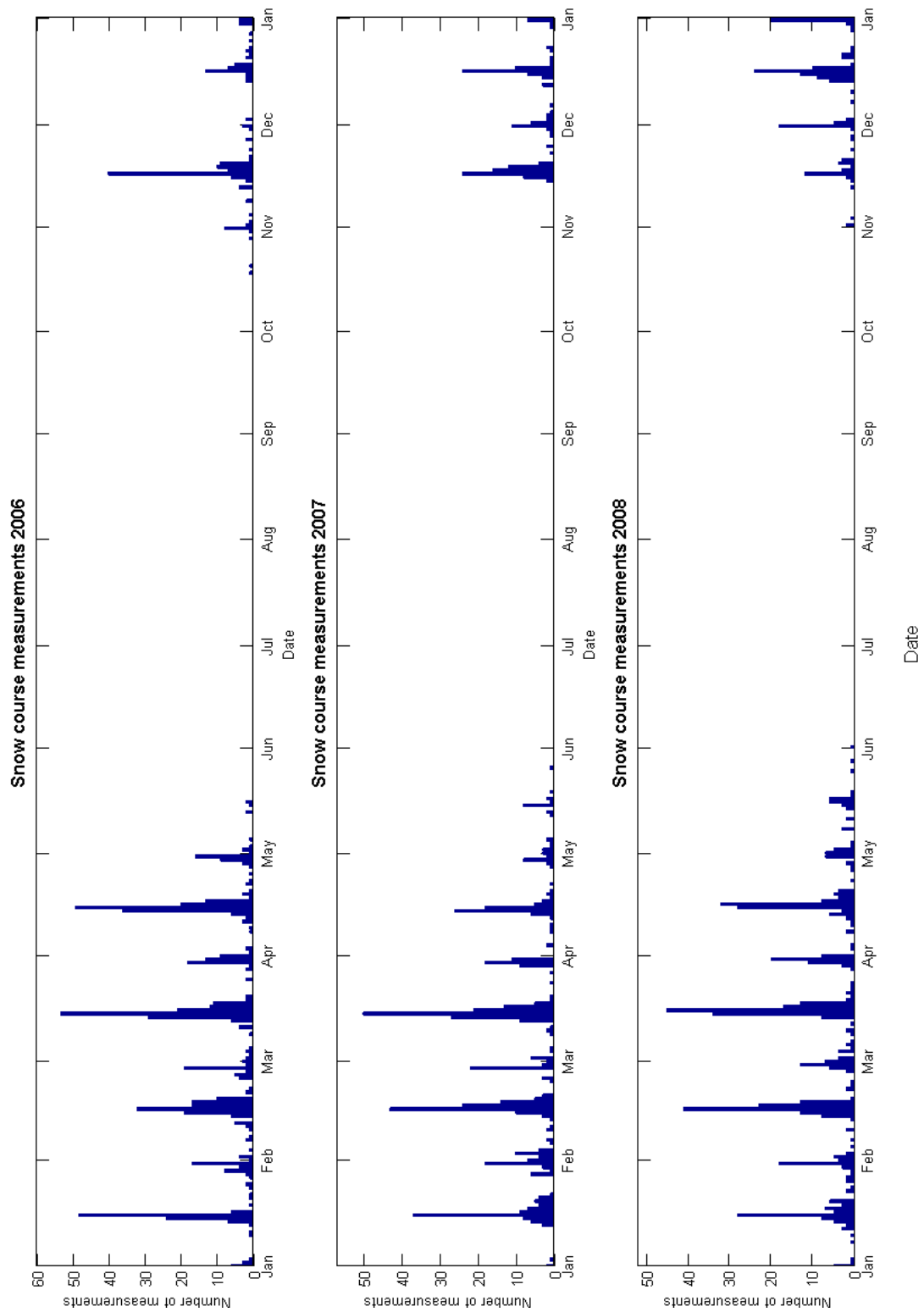


Figure 3.6: Number of snow course measurements done on each day in spring 2006, 2007, and 2008.

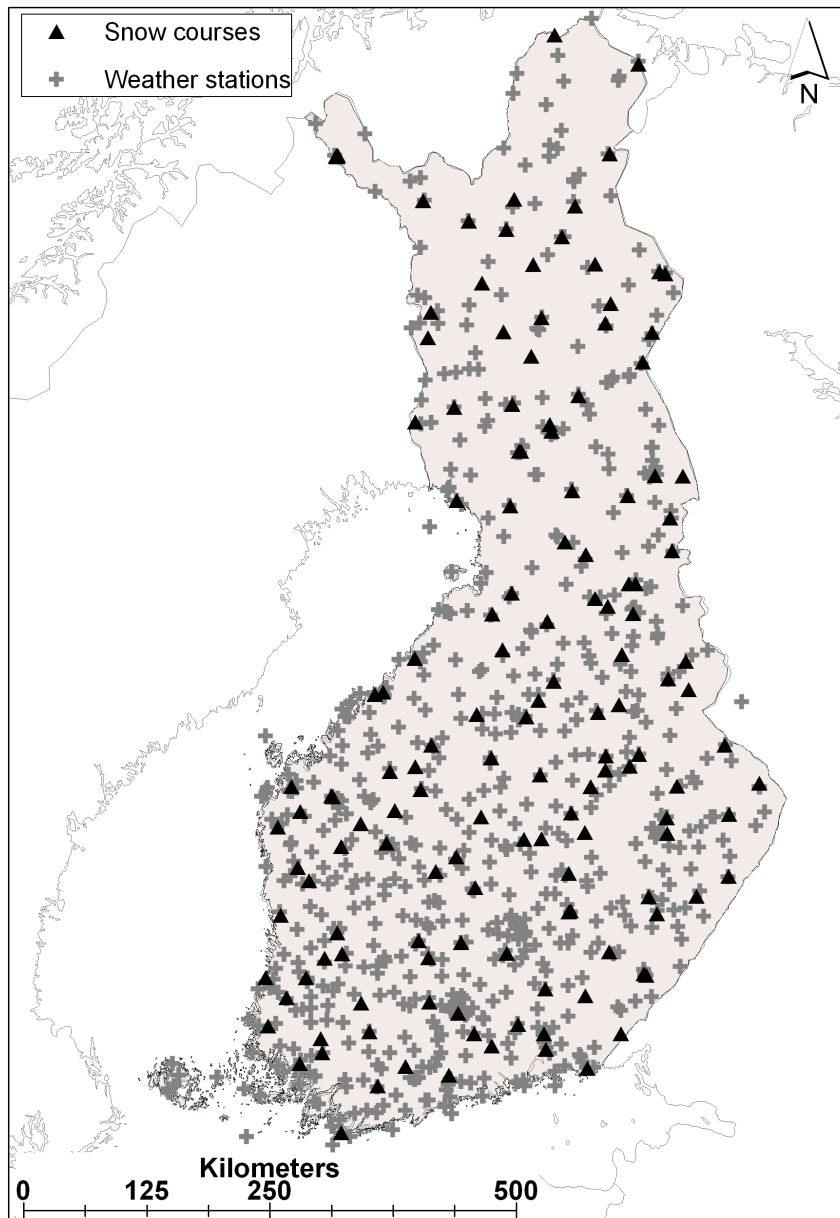


Figure 3.7: The locations of snow courses and weather stations in Finland [32].

model benefit from the accurate forest stem volume information. A newer map from SYKE (Figure 3.8) was used in SWE estimation described in Section 5.2.

A digital elevation model from the Land Survey of Finland was used for rectification of SAR images.

A drainage area map of Finland was used to calculate the average backscattering coefficient for each sub drainage area in [P III] and [P IV]. The map was provided by SYKE (see Figure 4.5).

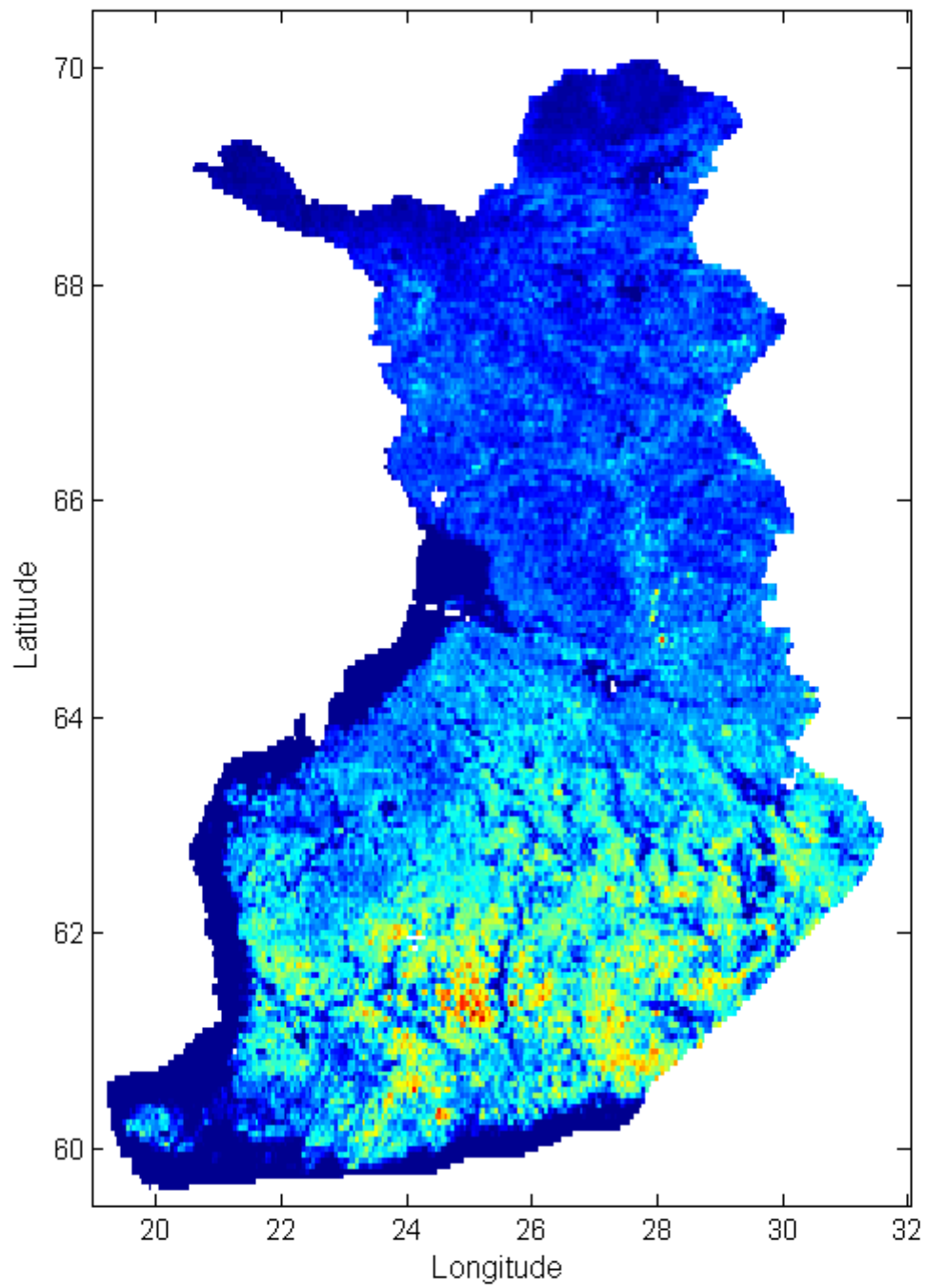


Figure 3.8: Forest stem volume in m^3/ha of Finland in 0.05° resolution. Produced by Pekka Härmä, SYKE.

4 Models

In the following, the models used in the work are presented.

Remote sensing models (also known as *forward models*) play important role when statistical inversion is employed. A remote sensing model describes the remote sensing observation as a function of geophysical parameters, like temperature, soil moisture or snow water equivalent.

Also the WSFS hydrological model is introduced, although it is not a remote sensing model *per se* but, rather an example of operational, dynamic environment model using multi-source data including parameters retrieved from remote sensing data (SCA and SWE).

The HUT emission model was used in [P II], the HUT forest backscattering model in [P III] and [P IV], the reflectance model in [P III], a simplified version of the WSFS model in [P IV], and a linear model in [P V].

4.1 Linear models

A linear model is the simplest type of a remote sensing model. It is of form

$$y = \beta_1 x + \beta_2 \tag{4.1}$$

where β_1 and β_2 are the model parameters. Usually they are the result from linear regression of remote sensing and reference data. An example of the linear model used in the work is the optical reflectance model.

4.1.1 Optical reflectance model

The optical reflectance model used in [P III] for snow covered terrain is in principle similar to microwave backscattering model. It can be written as a function of SCA as [32]

$$\rho(SCA) = (1 - t^2) \cdot \rho_{forest} + t^2[SCA \cdot \rho_{snow} + (1 - SCA) \cdot \rho_{ground}], \quad (4.2)$$

where ρ_{forest} , ρ_{snow} , and ρ_{ground} are reflectances of dense coniferous forest canopy, wet snow cover, and snow free ground, respectively. They have been determined empirically from the satellite data. t is forest transmissivity which is estimated from satellite-borne reflectance data. In practice, t varies from 0.26 to 1.0.

The model is employed with the NOAA/AVHRR data at visible band (580–680 nm) in which the effect of snow grain size is at its minimum [65]. It is used operationally at SYKE to estimate SCA during the spring time [32].

4.2 Nonlinear models

The radiative transfer model [4] is used commonly in remote sensing applications, for example for describing the effect of the atmosphere. It has the form of

$$y = ae^{2cx} + b(1 - e^{2cx}), \quad (4.3)$$

with three model parameters: a , b , and c .

The following microwave models are examples of the nonlinear models having properties of the radiative transfer model.

4.2.1 HUT snow emission model

The HUT snow emission model is a semi-empirical model describing the microwave emission of the snow covered land having forest canopy [46]. It takes into account the depth, grain size and density of the snow cover. It also takes into account the effects of atmosphere, forest cover and underlying soil. It describes the brightness temperature observed from space, T_B , as

$$T_B(\theta) = t(\theta) \cdot T_{B,gnd}(\theta) + T_{atm\uparrow}(\theta) + t(\theta) \cdot (1 - e_{gnd}(\theta)) \cdot (T_{atm\downarrow}(\theta) + t(\theta) \cdot 2.7K), \quad (4.4)$$

where t is the atmospheric transmissivity, $T_{B,gnd}$ the brightness temperature of ground scene, $T_{atm\uparrow(\downarrow)}$ the up(down)welling atmospheric brightness temperature, and e_{gnd} the emissivity of ground scene.

Next the ground scene is divided into forested and non-forested areas:

$$T_{B,gnd}(\theta) = f_{for} \cdot T_{B,for}(\theta) + (1 - f_{for}) \cdot T_{B,snow}(\theta), \quad (4.5)$$

where f_{for} is the forest coverage fraction, $T_{B,for}$ the brightness temperature of forested snow covered terrain, and $T_{B,snow}$ the brightness temperature contribution of snow and underlying terrain.

Assuming the temperatures of frozen ground, snow, and forest canopy be equal, and ignoring the scattering by forest canopy, the brightness temperature of the forested terrain is

$$T_{B,for} = (1 - t_{can}^2(1 - e_{snow})) \cdot T_{phys}, \quad (4.6)$$

where t_{can} is the transmissivity of the forest canopy and e_{snow} the emissivity of the snow covered terrain.

Finally, the transmissivity of forest canopy is modelled using empirical formulas

based on HUTRAD scatterometer measurements [20]:

$$t_{can} = t(f, \infty) + (1 - t(f, \infty)) e^{-0.0035 \cdot V}, \quad (4.7)$$

where $t(f, \infty)$ is $t(\infty, \infty) + (1 - t(\infty, \infty))e^{-0.028 \cdot f}$; $t(\infty, \infty) = 0.42$; f frequency in GHz, and V is the forest stem volume in m^3/ha .

Figure 4.1 describes model behaviour in two respects: diagram at the top shows predictions for snow pack emissivity as a function of frequency for four different SWE values and the diagram at the bottom shows the brightness temperature as a function of SWE for the AMSR-E frequencies calculated using the model implemented by FMI [25].

Figure 4.2 shows the model behaviour for two important parameters for AMSR-E frequencies: the top diagram shows the snow pack brightness temperatures as a function of snow grain size and the bottom one as a function of forest stem volume.

4.2.2 HUT forest backscattering model

The HUT forest backscattering model is a semi-empirical model, which describes the average backscattering coefficient of forested terrain as a function of forest stem volume. It is based on the equation of radiative transfer, its 0th order approximation (so called Cloud Model). However, since the parameters of the model are determined from empirical measurement data, they include the effects of the multiple scattering. The model parameters have been determined for C and X-bands, but they could be determined for other bands also. The forest stem volume range is from 0 to 300 m^3/ha . The valid incidence angle range is at least from 20 to 40 degrees.[47]

The backscattering coefficient σ^o is written as a function of forest stem volume V ,

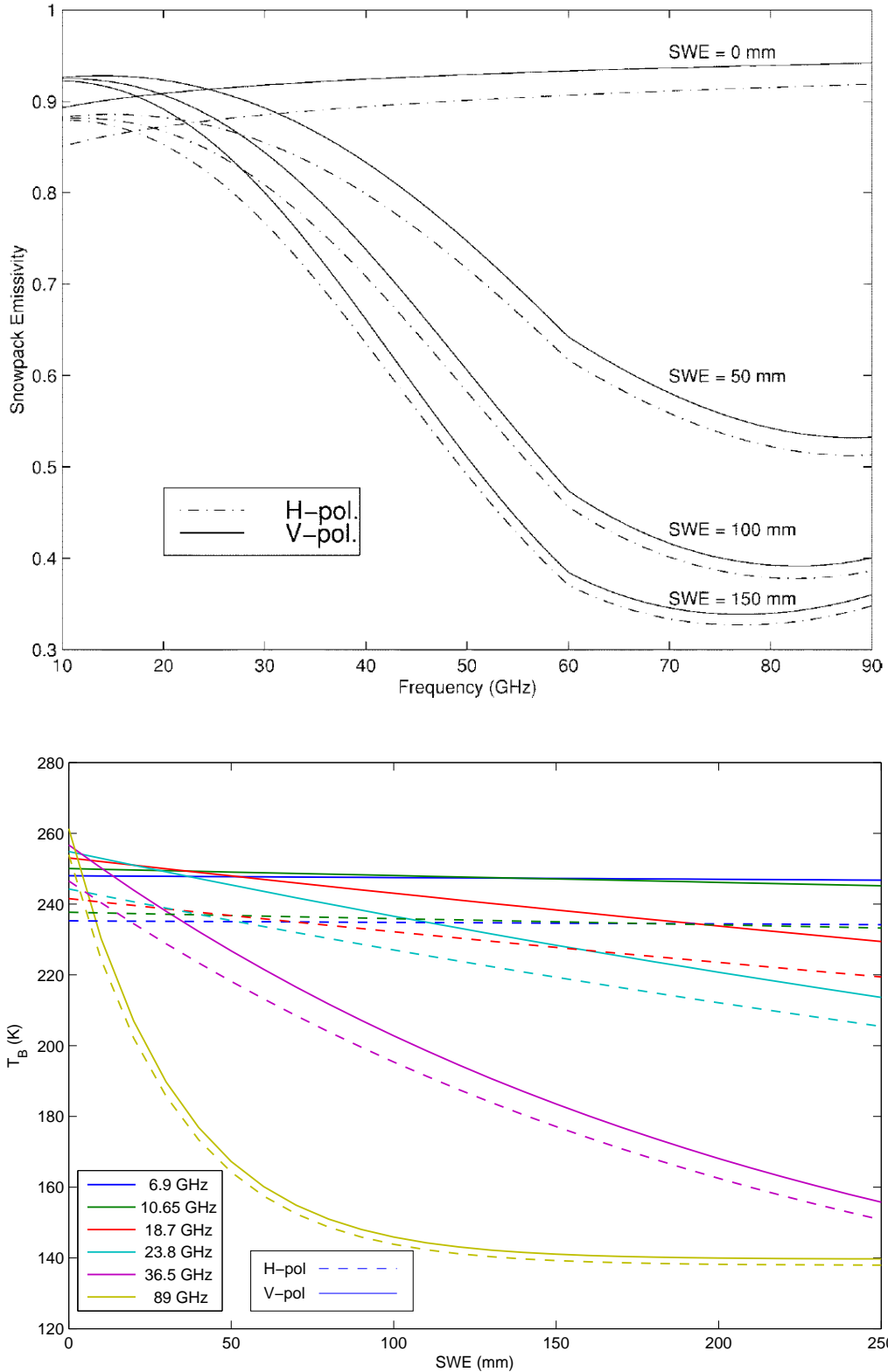


Figure 4.1: HUT snow emission model prediction for emissivity of snow covered terrain [46] (top) and brightness temperatures as a function of SWE (bottom). The model input parameter values were: nadir angle 53.1° ; density of snow 0.23 g/cm^3 ; snow grain size 1.0 mm; snow and soil temperature -10°C ; RMS soil surface height 2.5 mm; and soil permittivity 6-1j.

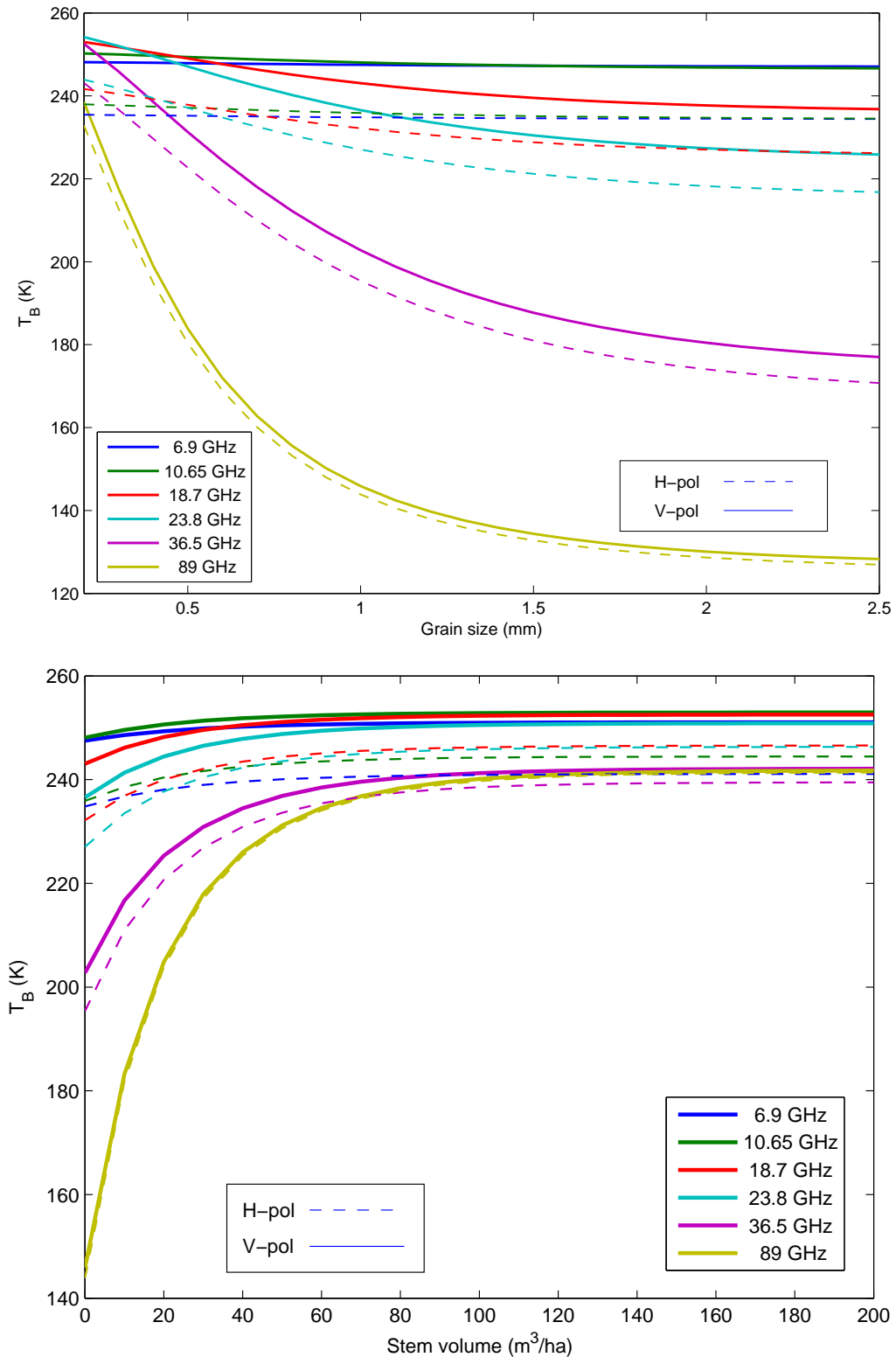


Figure 4.2: HUT snow emission model estimation of brightness temperatures of snow covered terrain as a function of snow grain size (top) and as a function of forest stem volume (bottom). The model input parameter values were: nadir angle 55° ; density of snow 0.23 g/cm^3 ; snow and soil temperature -10°C ; SWE 100 mm; RMS soil surface height 3 mm; and soil permittivity 6-1j. At the bottom figure, the snow grain size was 1.0 mm.

scalar variable χ , and the incident angle θ [48]:

$$\sigma^o(V, \chi, \theta) = \sigma_{can}^o(V, \chi, \theta) + t^2(V, \chi, \theta) \cdot \sigma_{surf}^o. \quad (4.8)$$

The backscattering of forest canopy σ_{can}^o is approximated by the following equation derived originally from ERS-1/2 observations [44] and later adjusted for RADARSAT-1 data:

$$\sigma_{can}^o(V, \chi, \theta) = p_2 \cdot \chi \cdot \cos \theta (1 - t^2), \quad (4.9)$$

where θ is the incident angle of the measurement and $p_2 = 0.099$ for C-band HH-polarisation (RADARSAT-1) and $p_2 = 0.131$ for VV-polarisation (ERS-1 SAR). Variable χ is a scalar reflecting the moisture content and freezing status of the forest canopy which must be solved for the particular weather conditions from the observed backscattering coefficients. For an example of that, see [28, p. 19].

Figure 4.3 depicts the contributions of different backscattering mechanisms to the total backscattering coefficient.

The two-way forest transmissivity t^2 is [47]:

$$t^2(V, \chi, \theta) = \exp\left(\frac{p_1 \chi V}{\cos \theta}\right), \quad (4.10)$$

where $p_1 = -4.86 \cdot 10^{-3}$ for C-band HH-polarisation and $p_1 = -5.12 \cdot 10^{-3}$ for VV-polarisation. See Figure 4.4 for an example of the transmissivity behaviour of forest canopy as a function of stem volume at 5.4 GHz.

To use the above described model in SCA determination, the SCA fraction should be included in the equation (4.8)

$$\sigma^o(V, \chi, SCA) = [SCA \cdot \sigma_{snow}^o + (1 - SCA) \cdot \sigma_{ground}^o] \cdot t^2(V, \chi) + \sigma_{can}^o(V, \chi), \quad (4.11)$$

where σ_{snow}^o is the backscattering coefficient of snow covered ground and σ_{ground}^o is that of snow-free ground surface.

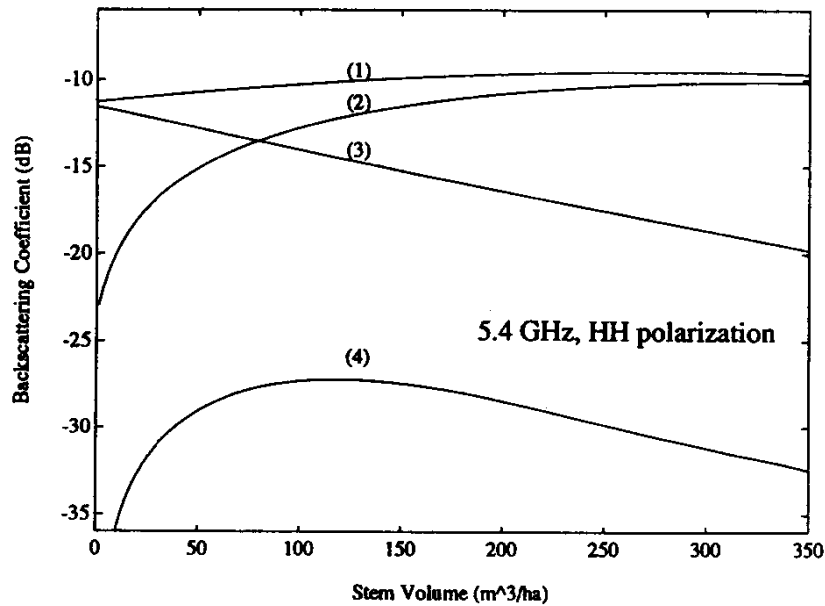


Figure 4.3: Backscattering contributions at 5.4 GHz, HH polarisation, 23° angle of incidence. (1) is the total backscattering coefficient, (2) is the canopy backscattering contribution, (3) is the soil backscattering contribution, and (4) is the trunk-ground corner reflection.[47]

The method requires these reference values for backscattering coefficient for the 100% wet snow cover and totally snow-free conditions.

4.3 Dynamic models

As an example of the dynamic environment model discussed in Section 2.3 is an operational hydrological model, which is presented next.

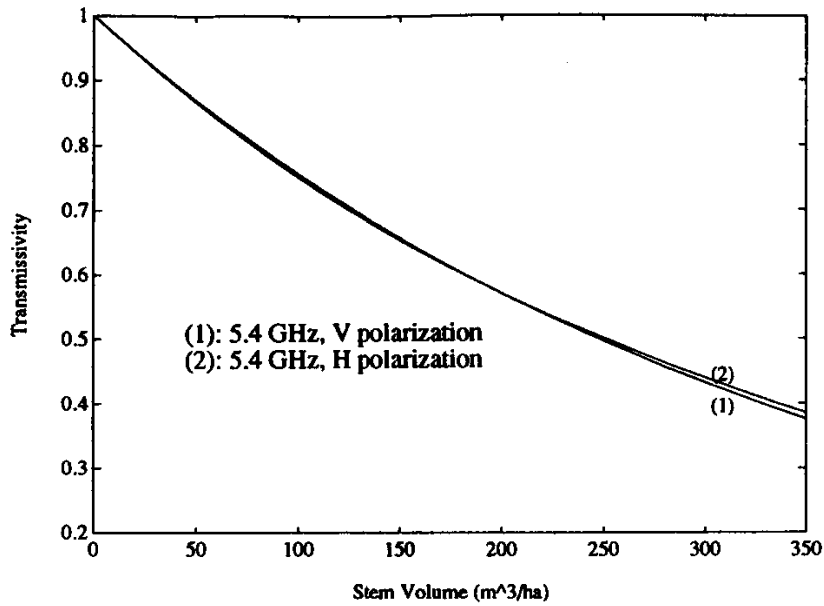


Figure 4.4: Forest canopy transmissivity estimated from HUTSCAT measurements for 5.4 GHz channel. The angle of incidence is 23° . [47]

4.3.1 Watershed Simulation and Forecasting System

The Watershed Simulation and Forecasting System (WSFS) is a hydrological model that covers the whole Finland [62] including cross-border watersheds, total area of 390 000 km². It is a real-time model that is run operationally at SYKE (Finnish Environment Institute). It is based on the HBV-model [3] and it uses sub drainage areas as calculation units (see Figure 4.5). The total number of sub drainage areas in the model is about 6 200.

The WSFS model is fed with a lot of measurement data continuously: meteorological data from 179 precipitation and 54 real time temperature stations, and weather radar precipitation information. The model is also updated against 487 water level and discharge stations, snow covered area (SCA) estimates from satellite data, and 158 snow courses measured once or twice per month [63].

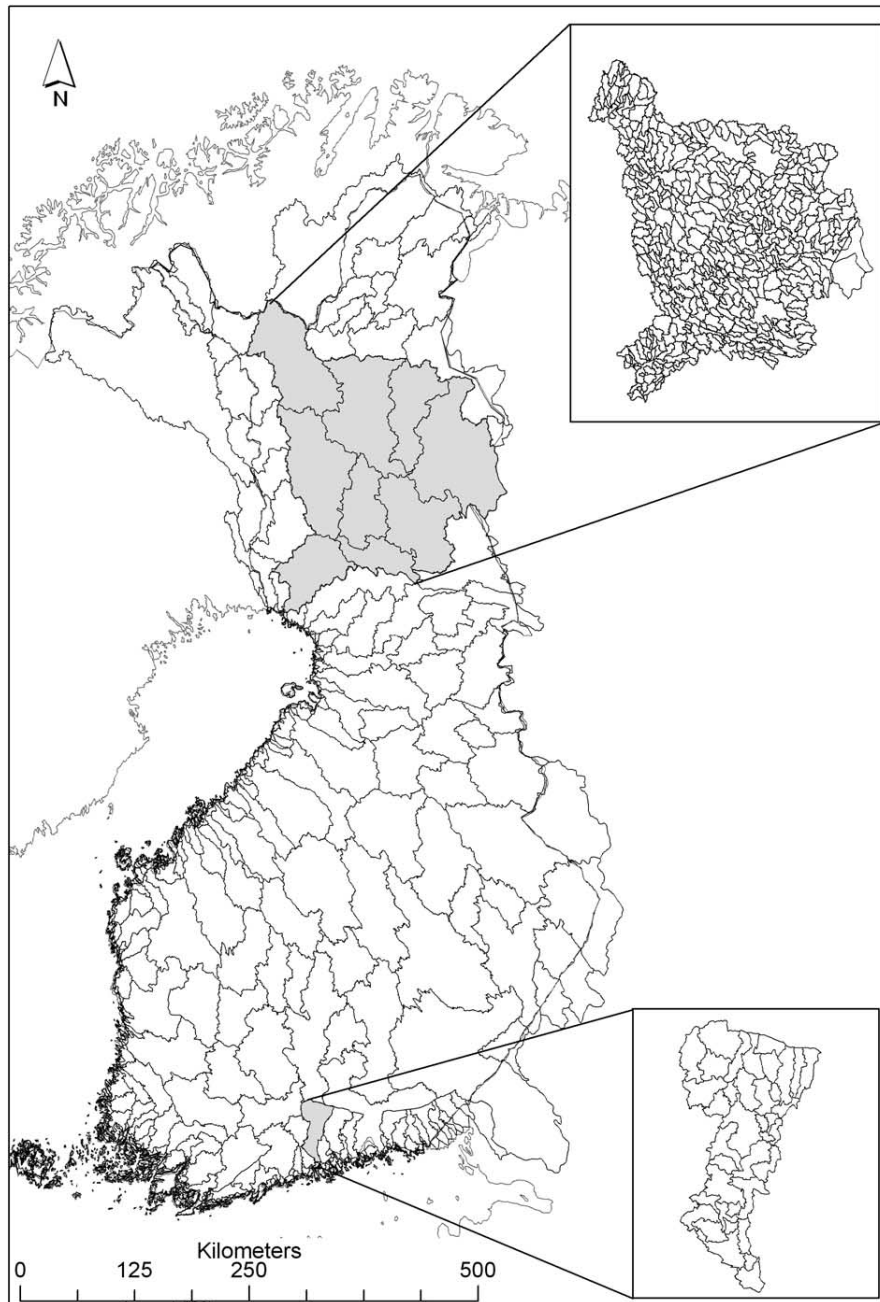


Figure 4.5: Drainage areas of Finland that the WSFS uses [32]. The map shows the level 1 drainage areas and the images on the right the level 3 drainage areas. Note that some drainage areas cross the Finnish border.

The model forecasts the discharge of the rivers and the corresponding water levels of both rivers and lakes. Figure 4.6 shows an example of a river discharge and water level forecast of the model. The model produces daily over 1000 discharge and water level predictions.

In order to better forecast floods in the spring time, the model needs more detailed information on the snow melting progress. The snow water equivalent (SWE) and snow covered area (SCA) are the two most important parameters for the model that can be retrieved from remote sensing data.

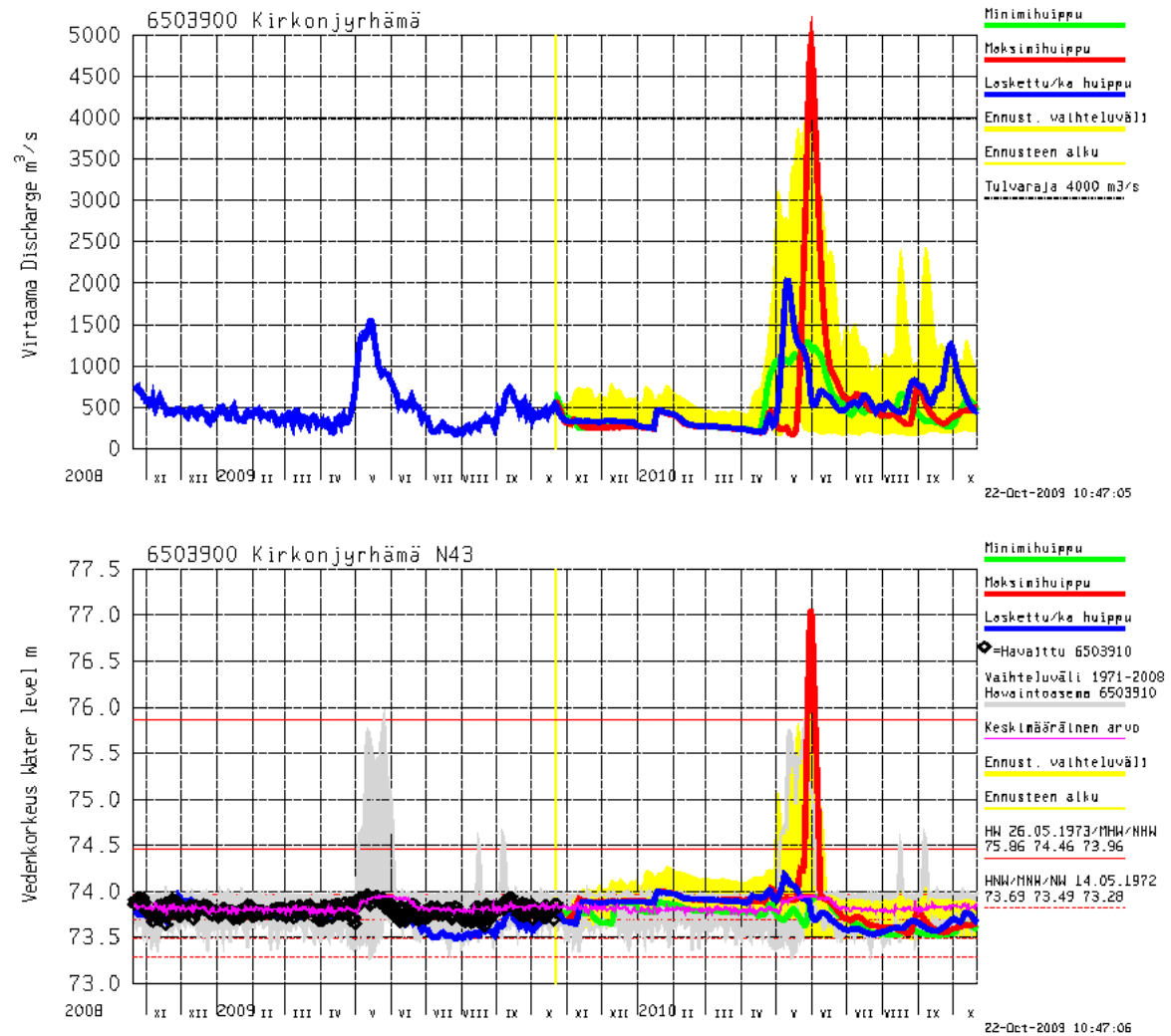


Figure 4.6: Example of river discharge (top) and water level (bottom) forecast of the WSFS model for river Kemijoki done at Oct 22nd, 2009. The yellow vertical line shows where the forecast begins. The thick red line denotes the maximum and green line the minimum, and the blue line the estimated/average peak. The variations of the forecasts and observed values are depicted in yellow and grey area, respectively. Source: SYKE

5 Methodology testing, results and discussion

In this chapter various ways of statistical inversion studies done in this work are presented. Also the main results of each study are presented.

5.1 Statistical inversion method

The inversion method presented in [P I] is based on the statistical inversion approach introduced in Chapter 2.2 and in [23]. A software application that contains several published microwave emission models and inversion algorithms, and a statistical inversion procedure was implemented by the author. It was targeted to a multi-channel microwave radiometer MIMR (Multi-Frequency Imaging Microwave Radiometer) that was planned by ESA in 1990's [31].

The software was used to test the inversion algorithms and the statistical inversion method when system noise was added to the simulated brightness temperature values. It was also used to test the applicability of the statistical inversion to different application areas, i.e. snow covered land, vegetated land, ocean, and ice cover.

Emission simulation

The software simulates the apparent temperature of several targets using the equation

$$\begin{aligned}
 T_{a,p}(f, \theta) = & e_{s,p}(f, \theta) \cdot T_s \cdot t(f, \theta) + T_{a,atmos\uparrow} \\
 & + T_{a,atmos\downarrow}(1 - e_{s,p}(f, \theta)) \cdot t(f, \theta) \\
 & + 2.7(1 - e_{s,p}(f, \theta)) \cdot t^2(f, \theta),
 \end{aligned} \tag{5.1}$$

where

$e_{s,p}$ = surface emissivity,

T_s = temperature of the surface,

$T_{a,atmos\uparrow}$ = up-welling atmospheric apparent temperature,

$T_{a,atmos\downarrow}$ = down-welling atmospheric apparent temperature,

t = transmissivity of atmosphere,

p = polarisation,

θ = angle of incidence, and

f = frequency.

The software simulates the microwave emission from ocean, sea ice, snow-covered, and vegetation-covered land at the frequencies of the MIMR instrument. It contains the following emission models:

- Pandey's model [39] for ocean surface,
- HUT emission model [46] for snow-covered land,
- Kerr's model [19] for vegetation-covered land,
- constant values for different ice types [10].

Dielectric constant of soil was calculated using equations of Hallikainen [12]. Atmospheric emissivity and transmissivity was simulated using the MPM model by Liebe [26].

Inversion algorithms

The inversion algorithms for ocean, snow, sea ice and vegetation were obtained from literature. The inversion algorithms implemented were:

- Miller's algorithm [33] for ocean wind speed,
- Wilheit's algorithm [66] for rain rate over ocean,
- SPD algorithm [1] and Künzi's algorithm [21] for snow water equivalent,
- Swift's algorithm [56] for sea ice concentration,
- Lojou's algorithms [27] for ocean surface temperature and water vapour and liquid water content of atmosphere.

The statistical inversion algorithm implemented is a maximum likelihood inverse solver that uses nonlinear least-squares fitting method for fitting the model into the multichannel results. The minimising problem is the same as (2.10)

$$\text{Minimize } \sum_{i=1}^{12} \frac{1}{2\sigma_i^2} (g_i(x_1, x_2, \dots, x_n) - (T_a)_i)^2 + \sum_{j=1}^n \frac{1}{2\lambda_j^2} (\hat{x}_j - x_j)^2,$$

where

- g_i = model representing the apparent temperature at the i th channel,
- $(T_a)_i$ = apparent temperature at the i th channel, measured from space,
- x_1, \dots, x_n = model parameters including the geophysical parameters of interest,
- \hat{x}_j = average value of the j th model parameter (*a priori* information),
- λ_j = standard deviation of the j th parameter value,
- σ_i = standard deviation of the measurement noise of the i th channel.

The initial values for the model parameters x_1, x_2, \dots, x_n are obtained from previously mentioned inversion algorithms. The developed technique is a unified method for retrieval of the geophysical parameters of any surface type.

Statistical model for atmosphere

For the atmospheric transmissivity, a statistical principal component model is utilised. This model was developed for the MIMR frequencies using the measurements of Salo-

nen et al.[54]. The principal component model allows the reduction of the statistical atmospheric transmissivity behaviour in the model representing the measurement into only one free parameter. Thus (5.1) can be expressed (leaving the *a priori* term out for convenience) as

$$\text{Minimize } \sum_{i=1}^{12} \frac{1}{2\sigma_i^2} (g_i(x_1, x_2, \dots, x_n, \alpha, \gamma^1) - (T_a)_i)^2, \quad (5.2)$$

where

α = atmospheric profile factor that contains information about the pressure, water content, etc. about the atmosphere, and

γ^1 = scalar variable (value of the first atmospheric transmissivity principal component).

Simulation software

The software was implemented in UNIX environment using C language and it was ported also to MS-DOS. The software contains emission simulation and inversion modules. The emission simulation can entirely be skipped by reading the apparent temperature values from a file in order to use measurement data.

The software allows one to investigate the sensitivity of the inversion algorithms to system noise by using the Monte Carlo noise simulation. In this method random noise is added to the apparent temperature values after which the inversion is performed. Figure 5.1 shows a snapshot of the workstation screen showing the simulated apparent temperature values and the inversion result histograms of the program.

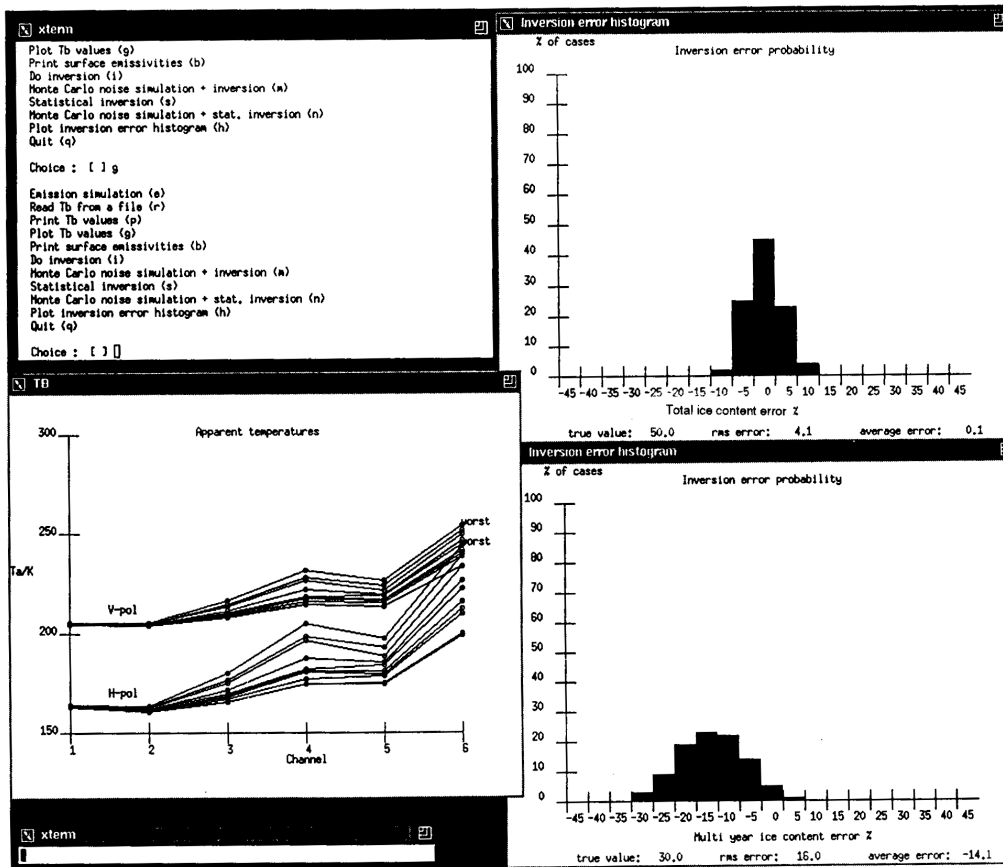


Figure 5.1: Windows of the simulation software showing emission calculation and a subsequent inversion. Apparent temperatures are calculated for sea ice at horizontal and vertical polarisations using the statistical atmosphere model. On both polarisations there are ten separate apparent temperature vectors corresponding to ten separate atmosphere transmissivity conditions.

Sensitivity analysis

Sensitivity analysis of the apparent temperature reveals the quantitative effects of different parameters affecting the measurement. Therefore, it is an essential part of developing the inversion techniques. Sensitivity is defined as

$$S = \frac{\partial T_a}{\partial x}, \quad (5.3)$$

where T_a is the apparent temperature and x is an affecting parameter.

An example of the sensitivity analysis is presented in Figure 5.2. The sensitivity is calculated using the HUT snow model and the following equation:

$$S_d = \frac{T_a(d = 0.4 \text{ mm}) - T_a(d = 1.2 \text{ mm})}{(0.4 - 1.2) \text{ mm}} \quad (5.4)$$

The result shows strong dependence of the apparent temperature to the grain size at 18.7, 36.5, and 89 GHz. The high sensitivity deteriorates the accuracy of snow water equivalent retrieval when the grain size cannot be estimated properly.

Results

The conventional inversion methods and the statistical inversion approach were tested in several applications using the developed simulation and inversion software. The statistical inversion method proved promising especially in ocean and sea ice applications. For land applications the greater number of free parameters made the inversion more difficult. One novel feature developed was the reduction of the atmospheric parameters with a statistical model for the MIMR frequencies.

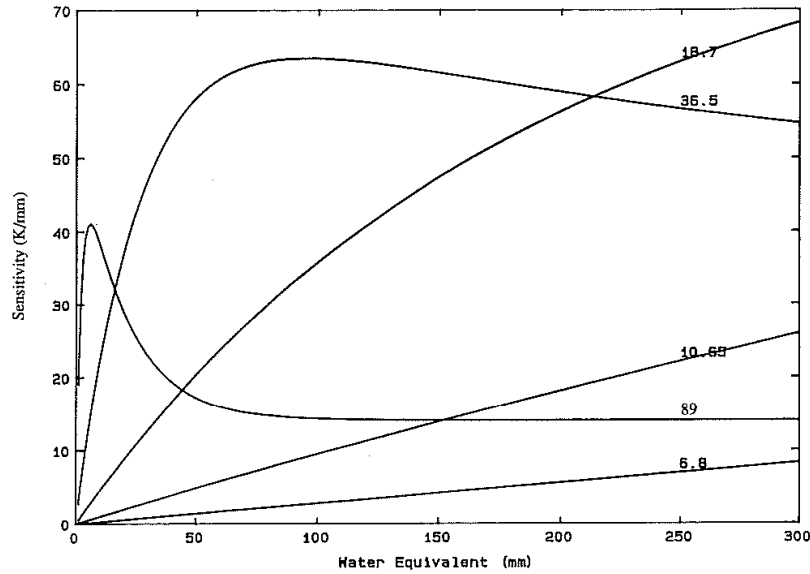


Figure 5.2: Sensitivity of the satellite observed apparent temperature to the snow grain size as a function of snow water equivalent for MIMR frequencies at vertical polarisation.

5.2 Statistical inversion with a priori data

In the study of [P IV] an operational system for production of snow water equivalent (SWE) and snow depth maps over large areas, like the whole Eurasia, was presented. The system uses synoptic weather station measurements and microwave radiometer data to determine the snow water equivalent over the area. The novel feature of the system was that it combined satellite observations of brightness temperature with ground-based data applying a nonlinear Bayesian data assimilation technique. This makes it possible to get better accuracy characteristics than using either of the two data alone. The original method is published in [43]. Figure 5.9 depicts one example snow depth map.

The data set consisted of AMSR-E microwave radiometer data and snow depth measurement of weather stations. Microwave data used were L2A data which were

rectified to 0.25 degree grid covering the area of 0° to 180° E and 55° to 85° N.

The HUT snow emission model introduced in section 4.2.1 was used as a remote sensing model.

Since the emission model is sensitive to snow grain size, which is an unknown parameter, the synoptic weather station snow depth measurements are used to determine snow grain size at all weather station locations. These values are used to interpolate the effective grain size over the whole area using ordinary Kriging [7, pp. 105–143].

The snow depth measurements are also interpolated over the whole area using ordinary Kriging. This interpolated snow depth map is used in the inversion process.

To omit the effect of liquid water in the snow, possible wet snow areas are screened using a simple dry snow detection algorithm [11]

$$SD > 80 \text{ mm and } T_{37V} < 250 \text{ K and } T_{37H} < 240 \text{ K} \quad (5.5)$$

where $SD = 15.9(T_{19H} - T_{37H})$ [mm], and T_{19H} and T_{37H} are brightness temperature values of the 19 and 37 GHz horizontal polarisation channels.

The inversion process is not applied for areas having wet snow, instead the interpolated snow depth value is used as an estimate.

Figure 5.3 depicts the system showing inputs, background information, and the results. Input files consist of rectified radiometer files of 18 and 37 GHz at horizontal and vertical polarisations and snow depth measurements of weather stations. Background information consists of a forest stem volume map and a water mask. Output consists of SWE and SD estimation maps.

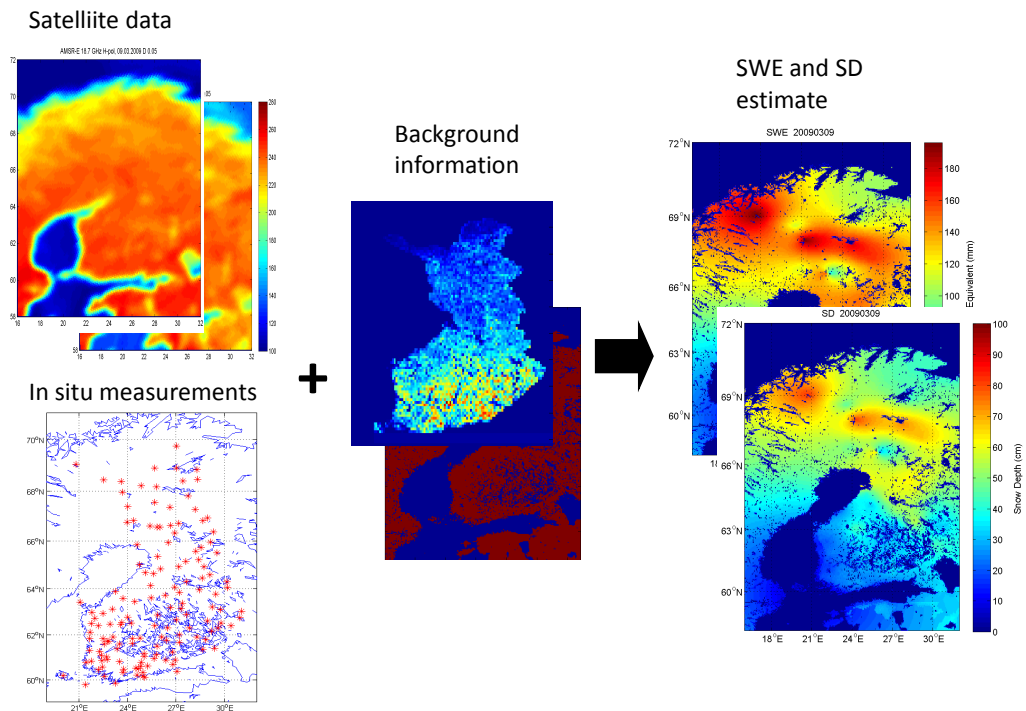


Figure 5.3: The SWE map production process showing input and output files.

Inversion process

First the modelled brightness temperature difference is fitted to the observed brightness temperature difference $T_{diff} = T_{18.7H} - T_{36.5H}$ using the snow grain size d_0 as a fitting parameter:

$$d_{0,ref} = \min_{d_0} (T_{diff} - f(\rho, D_{ref}, d_0))^2 \equiv 0, \quad (5.6)$$

where f is the HUT emission model, D_{ref} is the observed snow depth and ρ is the snow density ($SWE = \rho D$).

Next the snow depth for every pixel in the area is determined using inversion method. The method takes into account the statistical accuracies of the two data sources, i.e. the microwave radiometer and the weather station data, weighting the two data sources by their estimated variances.

The equation to be minimised has three terms when the previous estimates of snow depth (D_{t-1}) are available

$$\min_{D_t} \left(\frac{(T_{diff} - f(D_t))^2}{var(\varepsilon)} + \frac{(D_t - D_{ref,t})^2}{var(D_{ref})} + \frac{(D_{t-1} - D_t)^2}{var(D_t)} \right), \quad (5.7)$$

where

- $var(\varepsilon)$ is the variance of the modelling error,
- $var(D_{ref})$ variance of the snow depth measurements, and
- $var(D_t)$ is the day-to-day snow depth variance.

The flowchart of the inversion method is shown in Figure 5.4.

The error estimate for the method is also calculated using (2.13). An example of the error estimate map is shown in Figure 5.5.

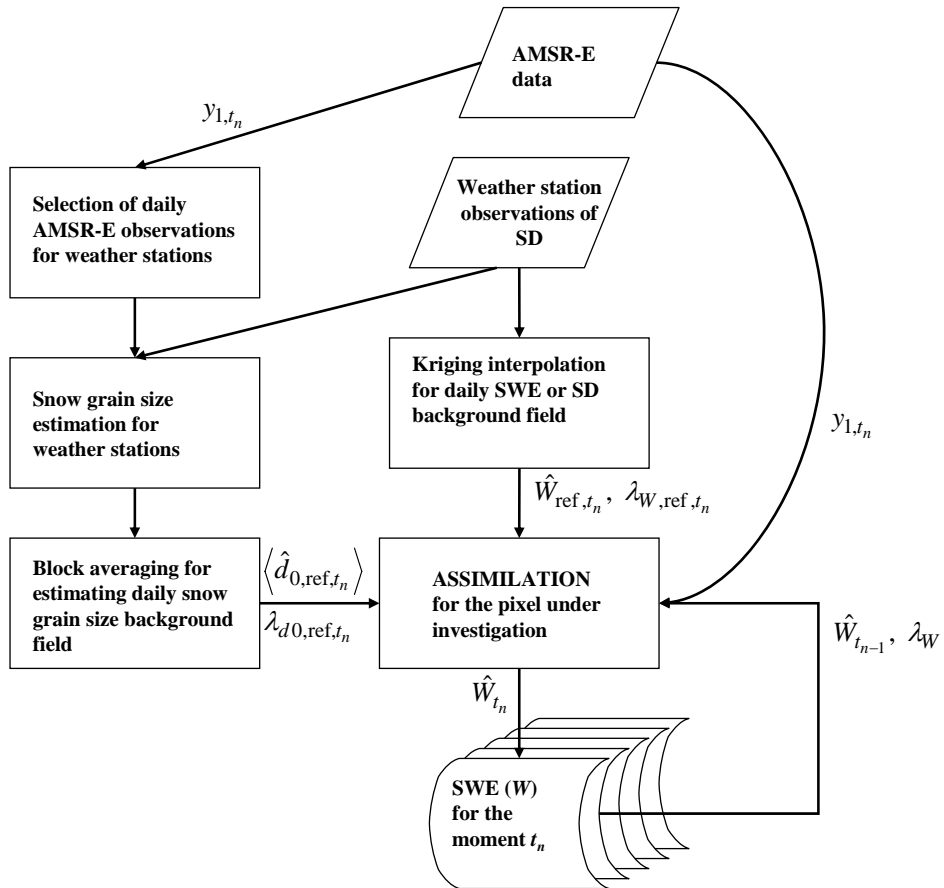


Figure 5.4: The flowchart of the SWE inversion method. [43]

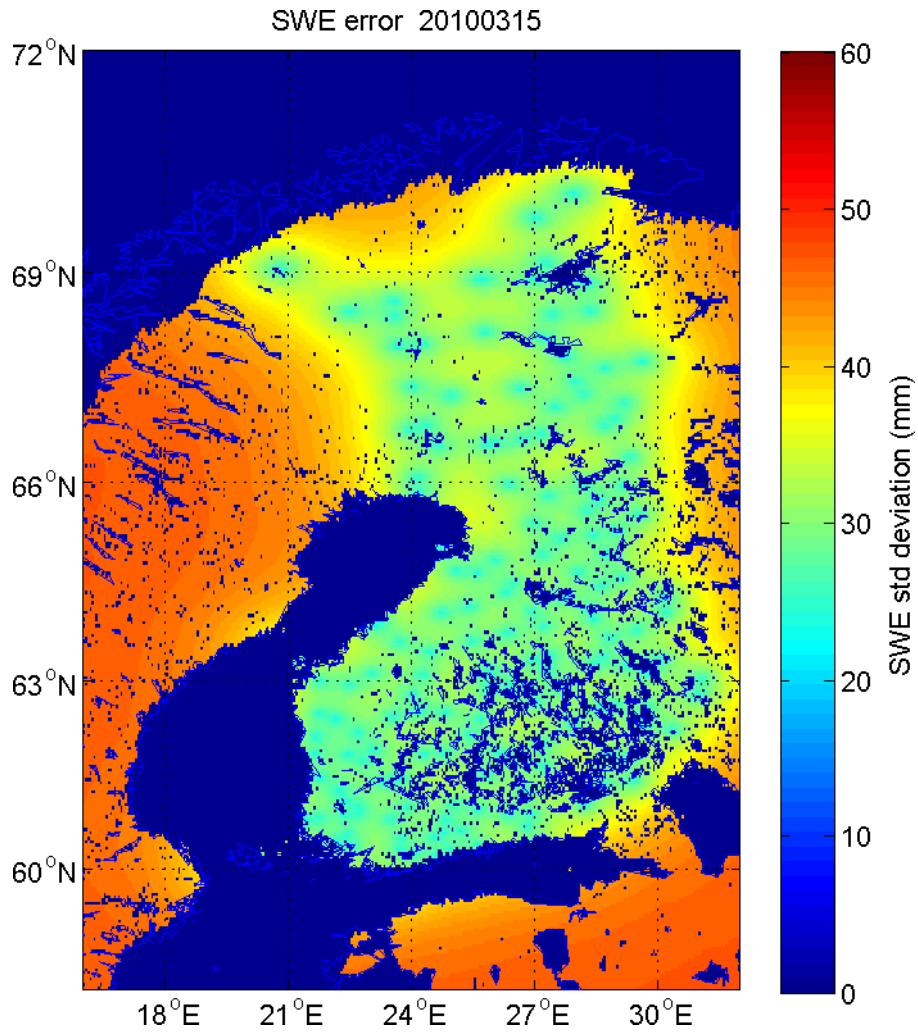


Figure 5.5: Standard deviation of the error of the SWE estimate. The error is smallest at the *in situ* data points ie. weather stations providing snow depth data.

Table 5.1: Statistics of snow course measurements on validation days.

	SWE	SWE	SWE	SD	SD	SD
	range	mean	median	range	mean	median
Date	mm	mm	mm	cm	cm	cm
2008-01-16	0–114	54	48	0–53	23	22
2008-02-16	1–165	81	71	2–70	30	22
2008-03-16	1–188	89	75	3–82	38	39
2008-04-16	0–223	77	37	0–90	39	42

Validation

The method has been validated in Russia by Takala [57] using Russian *in situ* measurements done on 1994–1997 (INTASS SCONE data). The main results are summarised in Figure 5.6. The method shows an rms error of 33 mm, and also it shows how the estimate begins to deviate from the measured value with SWE values larger than 100 mm.

The author has validated the method against snow course measurements done in Finland (see Section 3.3.2). The measurements of one course were averaged and the average value was compared to the snow depth or SWE estimate of the same location. Since the snow course measurements are not done exactly at the 16th of the month (see Figure 3.6) but also a day before or day after, also the measurements of one day before and after the estimation day were taken into account. Table 5.1 shows the statistics of the values of SWE and SD on validation points. Forest stem volume map of Finland produced by SYKE was used (see Figure 3.8).

Figure 5.7 shows the four SWE maps used in the validation.

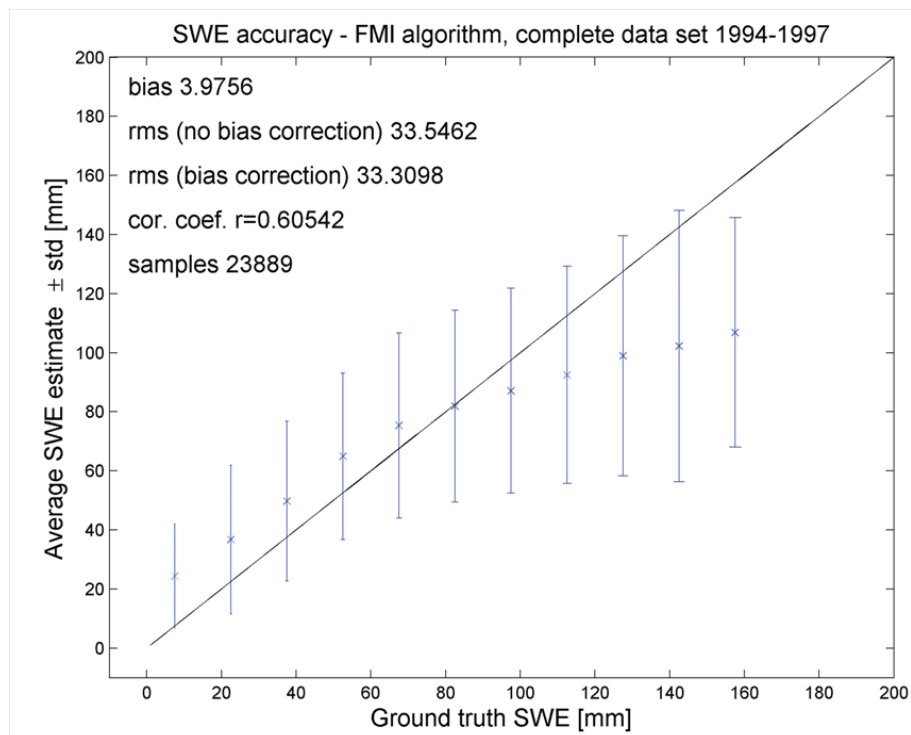


Figure 5.6: Scatter plot of SWE estimates vs. *in situ* measurements in Russia. Validation is done for winters 1994–97 using INTASS SCONE data. [57]

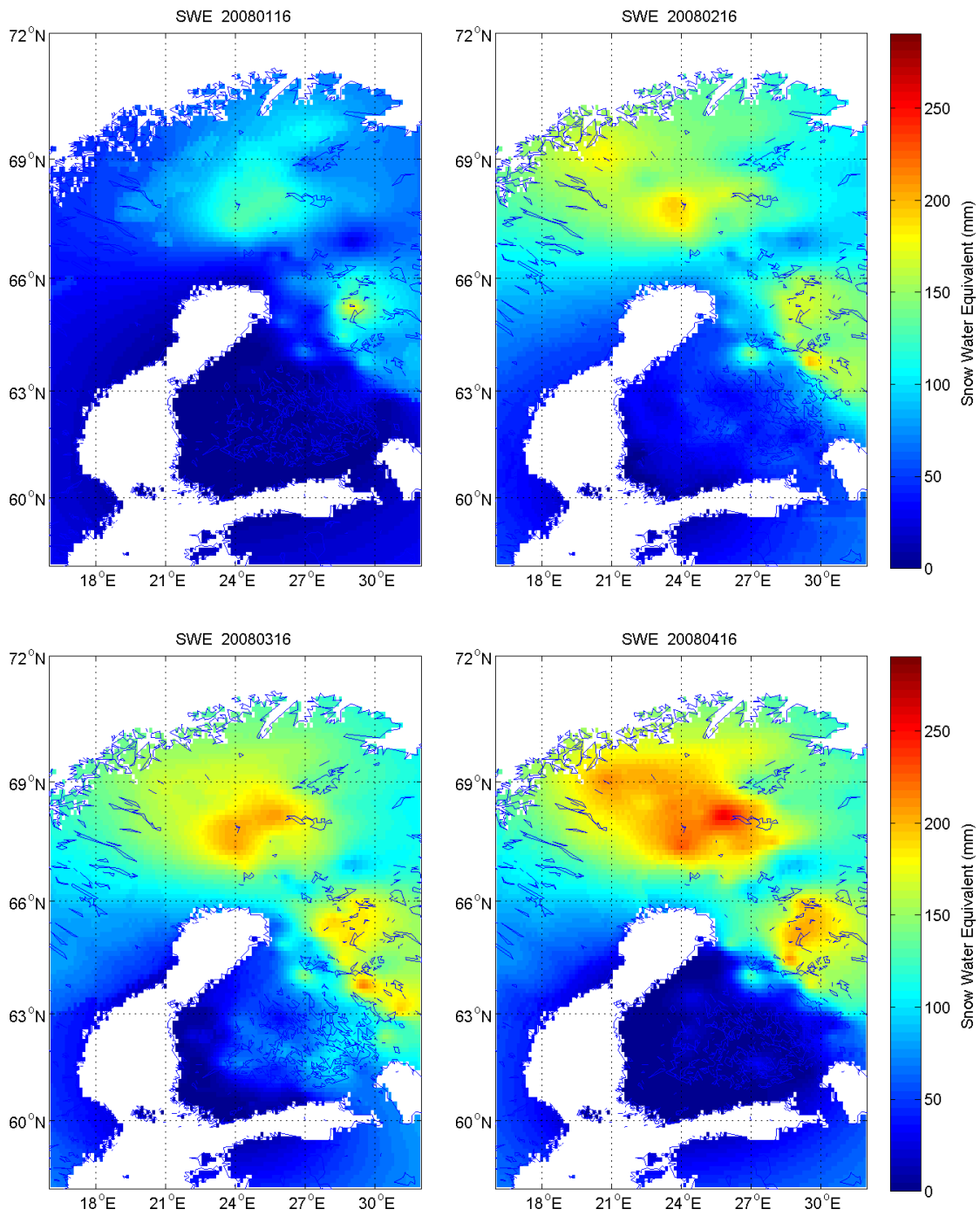


Figure 5.7: SWE estimations of Finland on 16th of January, February, March, and April 2008 in 0.125 degree resolution.

Table 5.2: Parameters used in the assimilation process.

Parameter	value
Snow density	0.24 g/cm ³
Variance of snow depth measurements	100 cm ²
Forest coverage fraction	77 %
Satellite orbit	descending (night time)
Grid	0.125 × 0.125 degrees
Area	16–32° E, 58–72° N

The parameters used in the assimilation process are presented in Table 5.2. The value for snow density in Finland varies in early winter from 0.21 to 0.27 g/cm³ increasing in late winter to 0.29–0.34 g/cm³ [51, p. 98]. However, a constant value of 0.24 g/cm³ was used for snow density.

Table 5.3 presents the results of the SWE validation and Table 5.4 results of the snow depth validation in spring 2008. Figure 5.8 shows the corresponding scatter plots of the results for SWE and snow depth.

These results show some over estimation (positive bias), which could possibly be reduced by tuning the modelling parameters. The accuracy is within the errors reported by others, in the range of 10–20 mm of SWE, even 30 mm or more [52]. Pulliainen has reported RMSE values of 9–13 cm in snow depth and 28–35 mm in SWE in his study [43], which is in line with the results obtained here.

Table 5.3: Validation results of the retrieved snow water equivalent against snow course measurements in spring 2008.

Date	Julian day	Snow	N	Unbiased			r
		course JD		RMSE (mm)	BIAS (mm)	RMSE (mm)	
2008-01-16	16	15–17	41	24	8	23	0.862
2008-02-16	47	46–48	77	27	16	22	0.902
2008-03-16	76	75–77	96	25	5	24	0.912
2008-04-16	107	106–108	68	32	-13	29	0.926
total			282	27	4	27	0.900

Table 5.4: Validation results of the retrieved snow depth against snow course measurements in spring 2008.

Date	Julian day	Snow	N	Unbiased			r
		course JD		RMSE (cm)	BIAS (cm)	RMSE (cm)	
2008-01-16	16	15–17	40	8.5	-1.3	8.4	0.892
2008-02-16	47	46–48	77	9.5	4.2	8.5	0.920
2008-03-16	76	75–77	71	10.3	3.0	9.8	0.912
2008-04-16	107	106–108	51	11.0	-1.8	10.8	0.943
total			239	9.9	1.7	9.8	0.923

Results

An operational system for estimating SWE and SD over large areas was developed and tested. SWE and snow depth maps covering the whole Eurasia were produced operationally for the winter 2007–2008 at FMI (<http://snow.fmi.fi>). The method is also used in Finnish Environment Institute (SYKE) covering the area of Finland to provide SWE data to the WSFS system.

5.3 Statistical inversion with two data sources

In the study presented in [P III] the SCA was retrieved from SAR data and from optical AVHRR data. While optical data is more accurate, it is lacking on some days due to cloudiness. Then the microwave radar still can provide SCA estimate.

The area used in the study was whole Northern Finland containing over 2000 sub drainage areas covering an area of 130 000 km².

The SAR data consisted of five RADARSAT wide swath images for spring 2004. The backscattering values were averaged into six classes based on the forest stem volume (open areas, 1–50, 51–100, 101–150, 151–200, over 200 m³/ha) for each sub drainage area.

The optical data used were NOAA AVHRR images from spring 2004. Reflectance values of AVHRR channel 1 (580–680 nm) were averaged to each sub drainage area.

Two remote sensing models were used: the HUT backscattering model introduced in Section 4.2.2 and the optical reflectance model introduced in Section 4.1.1.

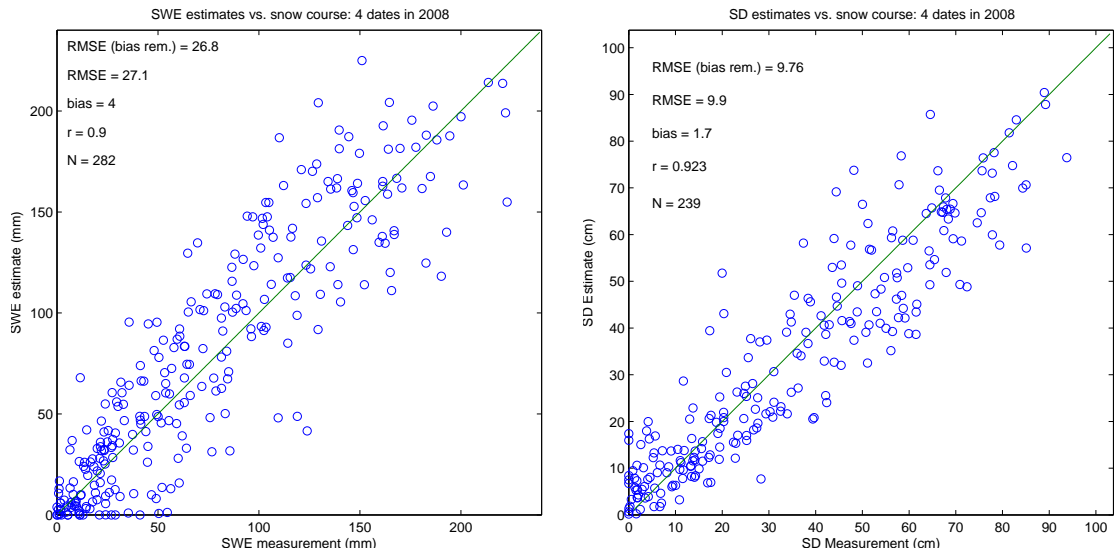


Figure 5.8: Scatter plots of the estimated SWE and SD versus snow course measurements for January 16th, February 16th, March 16h, and April 16th 2008.

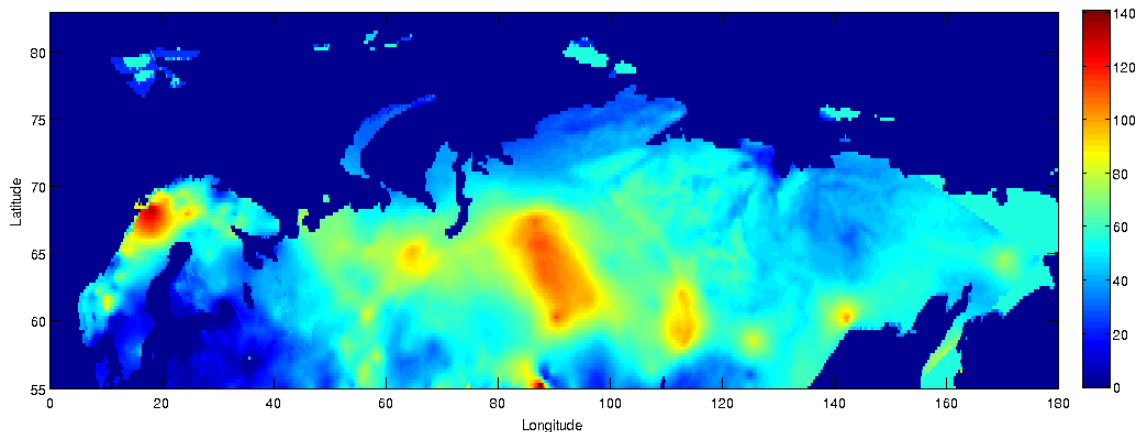


Figure 5.9: Snow depth map (in cm) over Eurasia on March 13th, 2007.

The inversion was performed using the equation (2.10) yielding in this case to:

$$\min_{SCA,a} J(\chi, SCA) = \min_{SCA,a} \sum_{i=1}^N w_1 (\sigma_{model,i}^o - \sigma_{SAR,i}^o)^2 + w_2 (\rho_{model} - \rho_{AVHRR})^2, \quad (5.8)$$

where $\sigma_{model,i}^o$ is the calculated and $\sigma_{SAR,i}^o$ the measured backscattering coefficient for the forest stem volume class i and N is the number of forest stem volume classes. Similarly, ρ_{model} is the calculated and ρ_{AVHRR} the measured reflectance of the sub drainage area. Weighting factors w_1 and w_2 represent the accuracy of the corresponding values inversely proportional to variance of the modelling error.

Figure 5.10 illustrates the iterative minimisation procedure.

Results

The SCA estimation was first performed using both AVHRR data and SAR data alone, and then using both data together. Figure 5.11 depicts visually the results of the SCA retrieval.

Figure 5.12 depicts the correspondence between SCA estimates retrieved from SAR and AVHRR instruments.

Currently the retrieval accuracy for SAR data is lower than for optical data: reported accuracies for the SAR method is 25 % units [29] versus 15 % units for the optical method [32].

When optical images are not available due to clouds, SAR data can be used to augment the SCA retrieval in these cases.

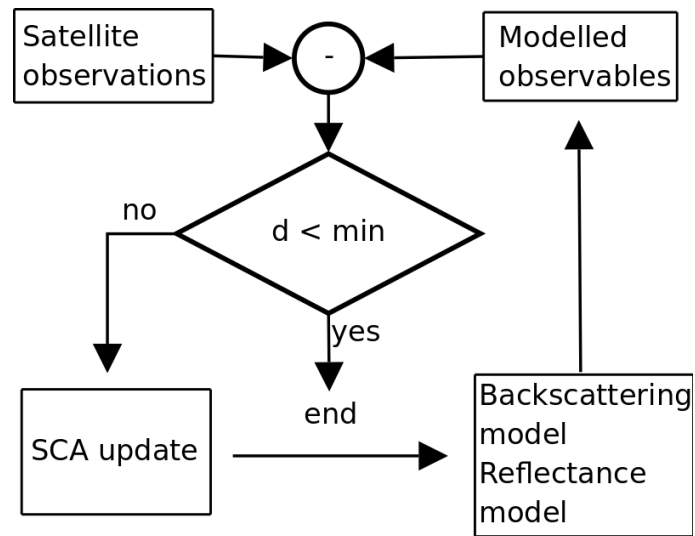


Figure 5.10: Flowchart of the retrieval of SCA from two remote sensing data sets: optical and SAR data.

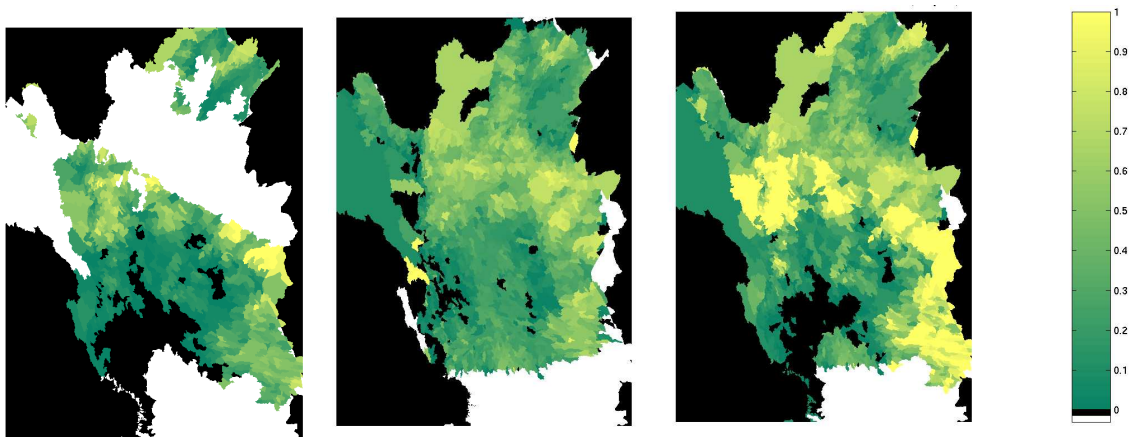


Figure 5.11: SCA derived from NOAA AVHRR data of May 5th, 2004 (left), from SAR data of May 6th (center), and from both data using statistical inversion (right).

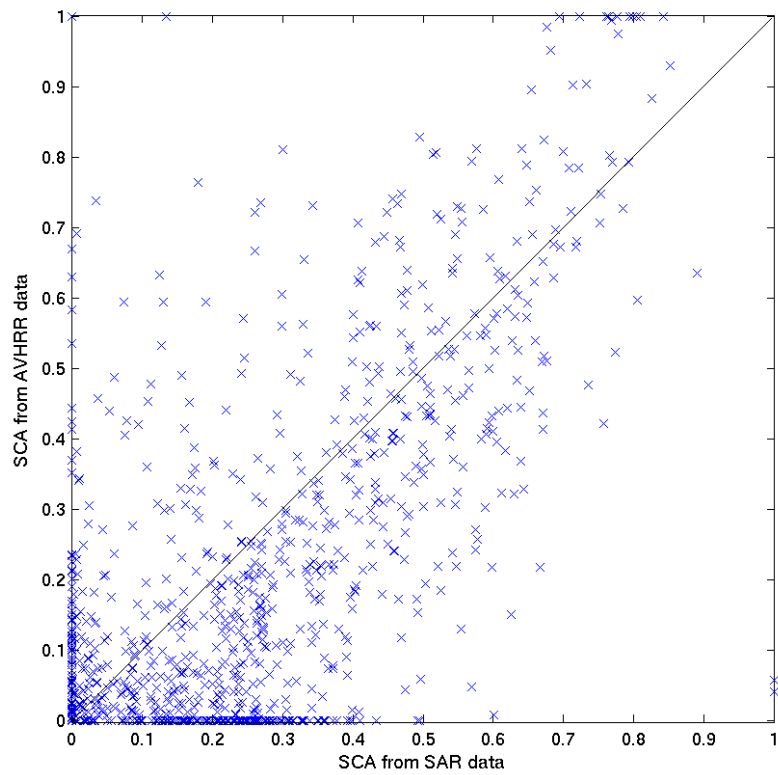


Figure 5.12: SCA derived from NOAA AVHRR data of May 5th, 2004 versus SCA from SAR data of May 6th, 2004. Correlation coefficient $r=0.66$ and $RMSE=0.197$.

5.4 Assimilating data into a dynamic model

In the study of [P IV] the SCA retrieved from SAR data were assimilated directly into the WSFS model.

The test area was in Northern Finland in river Kemijoki drainage area near lake Lokka (see Figure 5.13).

The satellite data consisted of 16 ERS-2 images from years 1997, 1998, 2000, and 2001. The backscattering values inside the 14 drainage areas (see Fig. 5.13) were averaged into five classes based on the forest stem volume. These average values were used in the inversion.

The models used in the inversion procedure were a simplified version of the WSFS model (see section 4.3.1) and the HUT forest backscattering model (see section 4.2.2).

The developed assimilation method can be described as follows: The hydrological model is optimised with respect to uncertain model state variables by applying a constrained iterative algorithm in which the difference between the the remote sensing model and remote sensing observations is minimised (statistical inversion using a maximum *a posteriori* likelihood method). The method takes into account the error characteristics of the hydrological and remote sensing models.

The hydrological model has two correction factors that can be adjusted historically: temperature and precipitation correction factors. These two factors have different effects on the model behaviour. Increasing the temperature accelerates the melting process (if done during the melting season) or shifts the beginning of the melting earlier. On the other hand, increasing the precipitation (if done before the melting season) increases the snow depth and the volume of the discharge. During the

assimilation process, both parameters can be used to drift the internal model state variable SCA to the direction that the measured SAR data points. The output of the model (discharge) behaves though quite differently in these cases.

The equation to be minimised was

$$J(\chi, z) = \sum_{i,j} w_1 (\sigma_{model}^o(i, j) - \sigma_{radar}^o(i, j))^2 + w_2 (SCA - SCA_{orig})^2, \quad (5.9)$$

where

z is either precipitation correction coefficient p or temperature correction factor ΔT , $\sigma_{model}^o(i, j)$ is the calculated backscattering coefficient for the forest stem class i (open areas, 1–50, 51–100, 101–150, 151–200, over 200 m^3/ha) of the sub drainage area j , $\sigma_{radar}^o(i, j)$ measured backscattering coefficient for the forest stem class i of the sub drainage area j ,

SCA is the internal state variable of the hydrological model with the modified parameter (p or ΔT), and SCA_{orig} the same variable initially. Weighting factors w_1 and w_2 represent the accuracy of the corresponding values.

Figure 5.14 depicts the iterative procedure used.

Results

Figures 5.15 and 5.16 depict two examples of the results of the procedure to the WSFS output. Both figures contain two diagrams: the left diagram depicts the river discharge and the right one the SCA state variable of the model. The discharge diagram shows three curves: measured discharge, forecasted discharge without assimilation, and forecasted discharge with assimilation.

Figure 5.15 shows how the assimilation has clearly enhanced the discharge forecast. In this case the model has been corrected using the precipitation correction. Figure



Figure 5.13: The 14 sub drainage areas near lake Lokka in Northern Finland.

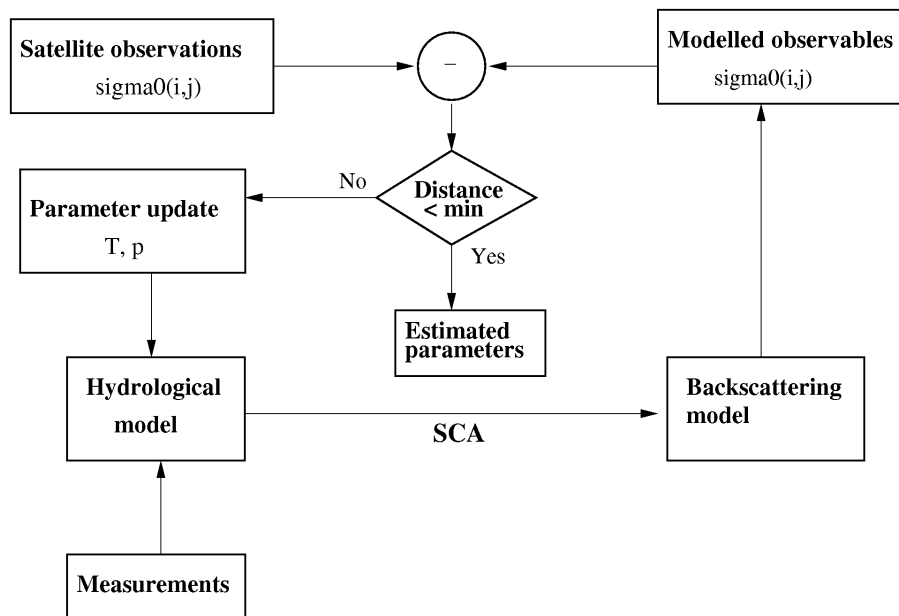


Figure 5.14: Flowchart of the assimilation of remote sensing data into the WSFS model.

5.16 shows the effect of the temperature correction: again the forecast has clearly moved towards the actual measured discharge.

5.5 A general statistical inversion tool

[P V] describes a tool for retrieving geophysical parameters that was developed by the author. The tool uses statistical inversion method presented in Chapter 2. The tool can be used by its own, or it could be integrated to a image processing system.

The tool supports linear models of type $y = \beta_1 x + \beta_2$ and one non-linear model: the radiative transfer model (2.4).

The usage of the tool is the following:

- Preparation of the field measurement data (reference data)
- Selection of the remote sensing model (type and parameters) either by knowing it beforehand or by using the learning phase
- Execution of inversion (analysis phase)
- Post processing the result

Usage example

In the example presented in [P V], forest stem volume was estimated from ERS INSAR coherence data. The coherence data was averaged for 210 forest segments of Southern Finland. The forest stem volume measurements were available for all the segments.

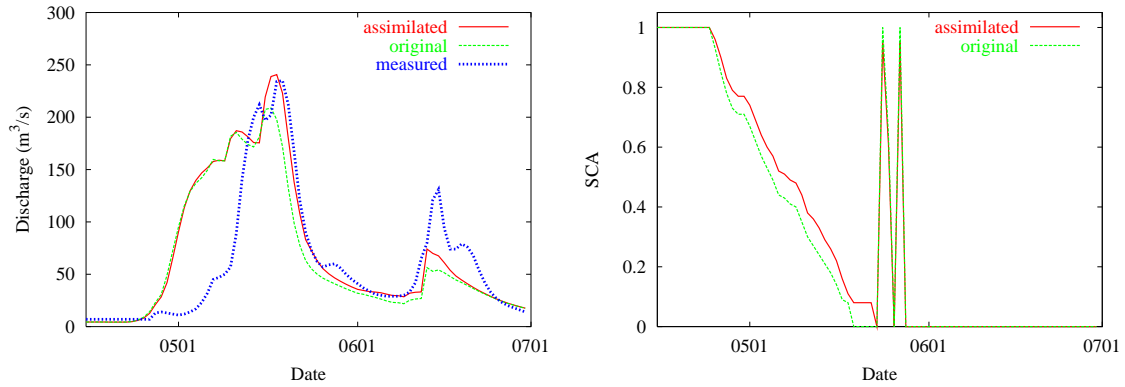


Figure 5.15: Left: Measured discharge, discharge from the model with and without the precipitation correction obtained from the assimilation procedure. Right: Corresponding SCA of the model (spring 1998).

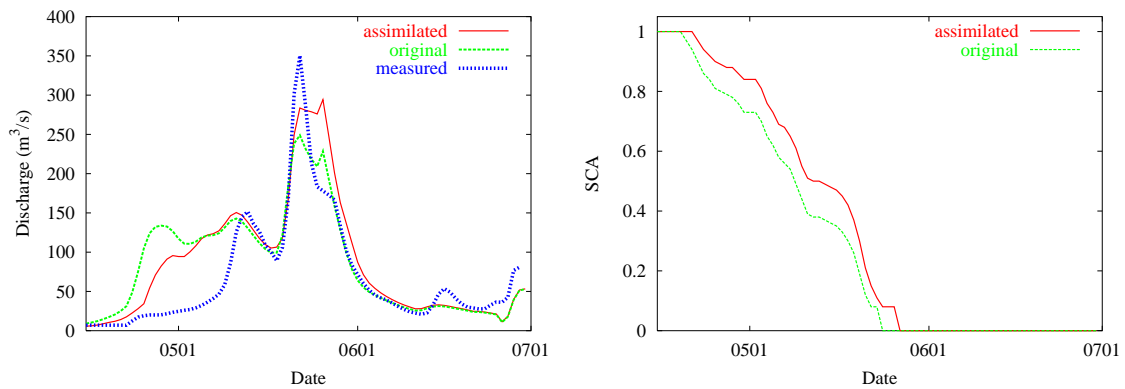


Figure 5.16: Left: Measured discharge, discharge from the model with and without the temperature correction obtained from the assimilation procedure. Right: Corresponding SCA of the model (spring 2000).

The remote sensing model was not known but it was determined conventionally by fitting a line to the data set (see Figure 5.17). That gave a linear model of

$$V = -0.000535 \cdot coh + 0.617,$$

where V is the stem volume in m^3/ha and coh the coherence value.

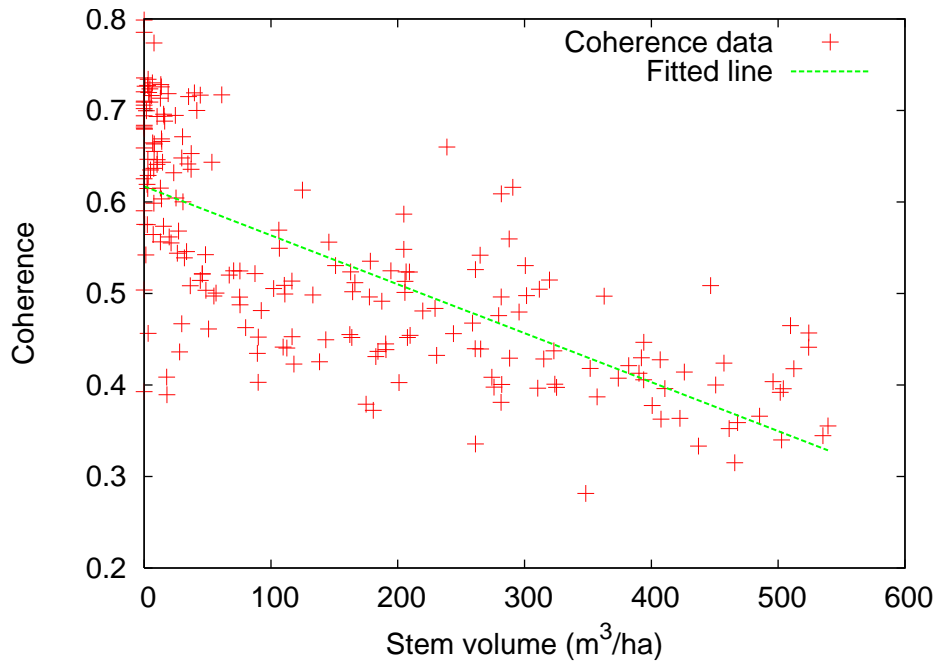


Figure 5.17: INSAR coherence data set versus forest stem volume data.

The statistical inversion tool described in [P V] was used to perform the inversion. Since the model in this case was linear, (2.11) and (2.12) were used by the tool. The accuracy (variance) of the measurement data was estimated to be 20 %. The results of the inversion are shown in Figure 5.18 with the estimated accuracies (variances).

Results

A general tool for retrieving geophysical parameters from remote sensing data was developed. It uses statistical inversion techniques, which means that the estimation

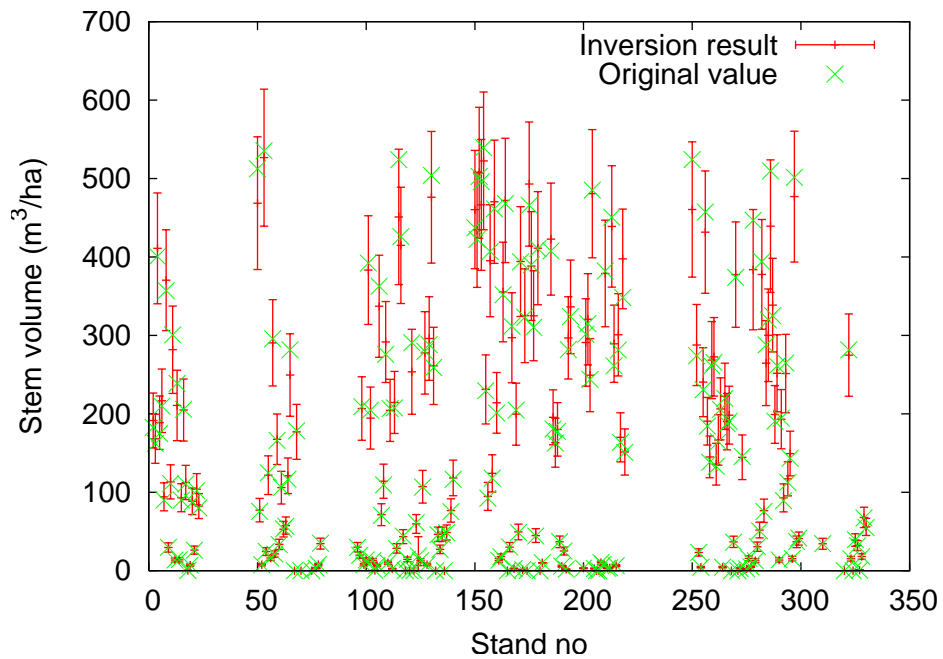


Figure 5.18: Forest stem volume estimations with error bars representing the accuracies.

results have also accuracy estimations. The developed tool is rather general, not tied to any particular application area. Since the program reads and writes the data using plain text files, it can be integrated to data processing chains. Also a prototype integration to a commercial image processing system was sketched.

5.6 Software

The work described in this thesis has been executed using different software tools in different computer systems running different operating systems. The computing environments, specific remote sensing software, software development tools, and documentation tools used are listed in the following.

5.6.1 Environment

Several different computing environments have been used to implement the software presented in papers [P I] to [P V].

The simulation software of [P I] was developed in UNIX environment (SunOS) and MS-DOS environment. The software for [P V] was developed for Windows XP environment, but was also compiled for Linux.

Systems described in [P II], [P III], and [P IV] were implemented on MATLAB. MATLAB, product of MathWorks, is a mathematical programming environment, that is currently available for Windows, Linux, Solaris, and Mac OS X. (<http://www.mathworks.com>)

5.6.2 Remote Sensing Software

- RADARSAT Swath Planner (for RADARSAT-1 image ordering)
- ERDAS IMAGINE (Image processing) <http://www.erdas.com>
- ER Mapper 6.4 in [P V]

5.6.3 Development Tools

Compilers

The software of [P I] was implemented using the C language, which is rather similar in both UNIX and MS-DOS environments. The graphics, however, are different in those environments, so they were done using different functions.

- SunOS: GCC (GNU C Compiler), X Window System
- MS-DOS: Borland C and its own graphics library

GNU C Compiler is available on wide range of operating systems: Windows, UNIX, and Mac OS X.

The statistical inversion software of [P V] was developed using the free Dev C++ programming environment (<http://www.bloodshed.net>). The Linux version was compiled using the GNU C++ compiler.

The system described in [P IV] contained a hydrological model component implemented in FORTRAN language. That part was compiled using GNU Fortran (G77) to a MATLAB mex-file. The mex-file is a special file that is possible to call from MATLAB code.

Libraries

A MATLAB add-on toolbox M-Map v1.4e (<http://www.eos.ubc.ca/~rich/map.html>) was used to produce figures of [P II].

Tools

CVS was used for source version control especially for program code of [P V].

SLOCcount was used to count the number of lines of the program code of [P V].

5.6.4 Documentation tools

Several documentation tools were used to write documentation and produce figures.

- \LaTeX (Document preparation system) [22]
- BibTeX (Reference management) <http://www.bibtex.org>
- L \AA X (Document processor) <http://www.lyx.org>
- DIA (Diagram drawing) <http://live.gnome.org/Dia>
- GIMP (GNU image manipulation program) <http://www.gimp.org>

6 Conclusions

In this work, the retrieval of geophysical parameters from remote sensing data using statistical inversion method was studied. The statistical inversion method was used in several different ways with different types of data. The application area was mainly snow, although the method is universal *per se*. The snow applications were selected because in that area Laboratory of Space technology has a lot of competence: it has developed both microwave remote sensing models and inversion algorithms for snow.

The remote sensing models play an important role on statistical inversion. Good models are essential in order to get good retrieval results. In this work, both microwave emission and scattering models, and an optical reflectance model were used. Remote sensing data were also assimilated into a dynamic environment model (WSFS). However, the method does not need a physical remote sensing model, the model can be determined from the remote sensing data conventionally, using for example regression. This approach was demonstrated in this work also.

One of the benefits of the statistical inversion method is that it automatically takes into account the statistical accuracy of the data used. If data from different accuracies are used, the method weights the different data optimally in the process. The method can also estimate the accuracy of the results based on the accuracy of the data and the models used.

The statistical inversion method was demonstrated with the following applications: snow water equivalent mapping in large areas (whole Eurasia) using microwave radiometer data, snow-covered area estimation of Northern Finland using optical and radar data together, and assimilating SCA retrieved from radar data directly into the watershed simulation system. Also the ERS INSAR data was used to

estimate the forest stem volume.

In addition to the studies mentioned above, two software applications were developed. The first one was developed to simulate brightness temperatures measured by a multichannel microwave radiometer and to test available inversion algorithms and the statistical inversion method. The other software application was developed as a statistical inversion tool that could be used either independently or as a component in an image processing system.

As a conclusion of the studies mentioned, the statistical inversion method is a feasible method for retrieving geophysical parameters from remote sensing data. The method is especially suitable for application where extensive measurement data are available to augment the remote sensing data.

References

- [1] Josef Aschbacher. 1990. Land surface studies and atmospheric effects by satellite microwave radiometry. Ph.D. thesis, University of Innsbruck, Austria.
- [2] Thomas Bayes. 1763. An Essay towards solving a Problem in the Doctrine of Chances. The Philosophical Transactions of the Royal Society 53, pages 370–418. URL <http://www.stat.ucla.edu/history/essay.pdf>. (accessed: May 20th, 2010).
- [3] Sten Bergström. 1976. Development and application of a conceptual runoff model for Scandinavian catchments. RHO Report 7, SMHI, Norrköping, Sweden.
- [4] Subrahmanyan Chandrasekhar. 1960. Radiative transfer. Dover publications, New York, USA. ISBN 0-486-60590-6, 393 pages.
- [5] B. J. Choudhury, T. J. Schmugge, A. Chang, and R. W. Newton. 1979. Effect of surface roughness on the microwave emission from soils. Journal of Geophysical Research 784, pages 5699–5706.
- [6] Committee on Earth Observation Satellites. 1989. Synthetic Aperture Radar Data Products Format Standard, 2.0 edition. URL <http://wgiss.ceos.org/archive/archive.pdf/sardata.pdf>. (accessed: May 20th, 2010).
- [7] Noel. A. C. Cressie. 1991. Statistics for spatial data. John Wiley & Sons, New York. ISBN 0-471-84336-9, 900 pages.
- [8] Roshanak Darvishzadeh, Andrew Skidmore, Martin Schlerf, and Clement Atzberger. 2008. Inversion of a radiative transfer model for estimating vegetation LAI and chlorophyll in a heterogeneous grassland. Remote Sensing of Environment 112, pages 2592–2604.

- [9] Michael S. Dawson, Adrian K. Fung, and Michael T. Manry. 1997. A robust statistical-based estimator for soil moisture retrieval from radar measurements. *IEEE Transactions on Geoscience and Remote Sensing* 35, no. 1, pages 57–67.
- [10] Preben Gudmandsen. 1990. Sea ice retrieval algorithm studies (Appendix F.2). In: Jouni Pulliainen (editor), *Study of Microwave Interaction with the Earth's Surface: Vol I Passive Microwave Remote Sensing*, pages 247–273. Helsinki University of Technology, Espoo, Finland. ESA Contract report 8447/89/NL/PB(SC).
- [11] Dorothy K. Hall, Richard E. J. Kelly, George A. Riggs, Alfred T. C. Chang, and James L. Foster. 2002. Assessment of relative accuracy of hemisphere-scale snow-cover maps. *Annals of Glaciology* 34, pages 24–30.
- [12] Martti T. Hallikainen, Fawwaz Ulaby, Myron C. Dobson, Mohamed A. El-Rayes, and Lin-Kun Wu. 1985. Microwave dielectric behavior of wet soil – Part 1: Empirical models and experimental observations. *IEEE Transactions on Geoscience and Remote Sensing* GE-23, no. 1, pages 25–34.
- [13] J. Michael Heneghan and Akira Ishimaru. 1974. Remote determination of the profiles of the atmospheric structure constant and wind velocity along a line-of-sight path by a statistical inversion procedure. *IEEE Transactions on Antennas and Propagation* 22, no. 3, pages 457–464.
- [14] Erich Hernandez-Baquero. 2001. Comparison of Statistical Inversion Techniques for Atmospheric Sounding. In: *Geoscience and Remote Sensing Symposium 2001 (IGARSS '01)*, volume 4, pages 1705–1707. IEEE.
- [15] JAXA. 2006. AMSR-E Data Users Handbook, 4th edition. URL http://www.eorc.jaxa.jp/en/hatoyama/amr-e/handbook_e.html. (accessed: May 20th, 2010).

- [16] Jari Kaipio and Erkki Somersalo. 2004. Statistical and Computational Inverse Problems, volume 160 of *Applied Mathematical Sciences*. Springer-Verlag, Berlin. ISBN 978-0-387-22073-4, 344 pages.
- [17] Juha-Petri Kärnä, Niina Patrikainen, and Jouni Pulliainen. 2005. Automatic rectification and calibration program for RADARSAT ScanSAR images. Report 61, Helsinki University of Technology, Laboratory of Space Technology, Espoo, Finland.
- [18] Toneo Kawanishi, Toshihiro Sezai, Yasuyuki Ito, Keiji Imaoka, Toshiaki Takeshima, Yoshio Ishido, Akira Shibata, Masaharu Miura, Hiroyuki Inahata, and Roy W. Spencer. 2003. The Advanced Microwave Scanning Radiometer for the Earth Observing System (AMSR-E), NASDA's Contribution to the EOS for Global Energy and Water Cycle Studies. *IEEE Transactions on Geoscience and Remote Sensing* 41, pages 184–194.
- [19] Yann Kerr and Eni Njoku. 1990. A semi-empirical model for interpreting microwave emission from semiarid land surfaces as seen from space. *IEEE Transactions on Geoscience and Remote Sensing* 28, no. 3, pages 384–393.
- [20] Nerijus Kruopis, Jaan Praks, Ali Nadir Aslan, Hanna M. Alasalmi, Jarkko T. Koskinen, and Martti T. Hallikainen. 1999. Passive Microwave Measurements of Snow-Covered Forest Areas in EMAC'95. *IEEE Transactions on Geoscience and Remote Sensing* 37, no. 5, pages 2699–2705.
- [21] Klaus F. Künzi, Subash Patil, and Helmuth Rott. 1982. Snow-Cover Parameters Retrieved from Nimbus-7 Scanning Multichannel Microwave Radiometer (SMMR) Data. *IEEE Transactions on Geoscience and Remote Sensing* GE-20, no. 4, pages 452–467.
- [22] Leslie Lamport. 1994. *LaTeX: A document preparation system*. Addison-Wesley, 2nd edition. ISBN 0-201-52983-1, 272 pages.

- [23] Matti S. Lehtinen. 1988. On statistical inversion theory. In: H. Haario (editor), *Theory and Applications of Inverse Problems*, number 167 in Pitman Research Notes in Mathematical Series, pages 46–57. Longman.
- [24] Juha Lemmetyinen. 2003. AMSR-E kaukokartoitusradiometrijärjestelmän L2A-tiedostojen käsittely. Avaruustekniikan erikoistyö, Helsinki University of Technology, Laboratory of Space Technology, Espoo, Finland. In Finnish.
- [25] Juha Lemmetyinen, Jouni Pulliainen, and Anna Kontu. 2009. HUT snow model multi-layer adaptation. Technical note, Finnish Meteorological Institute, Arctic Research Institute, Helsinki, Finland. Issue 1.1.
- [26] Hans J. Liebe. 1989. MPM - An atmospheric millimeter-wave propagation model. *International Journal of Infrared and Millimeter Waves* 10, no. 6, pages 631–650.
- [27] J.-Y. Lojou. 1990. Algorithmie et Methodes de Validation des Instruments en Radiometrie Hyperfrequence. Ph.D. thesis, University of Paris, France. (in French).
- [28] Kari Luojus. 2009. Remote Sensing of Snow-Cover for the Boreal Forest Zone using Microwave Radar. Ph.D. thesis, Helsinki University of Technology, Espoo, Finland.
- [29] Kari P. Luojus, Jouni T. Pulliainen, Sari J. Metsämäki, and Martti T. Hallikainen. 2006. Accuracy Assessment of SAR Data-Based Snow-Covered Area Estimation Method. *IEEE Transactions on Geoscience and Remote Sensing* 44, no. 2, pages 277–287.
- [30] Melinda C. Marquis, Richard L. Armstrong, Peter Ashcroft, Mary Jo Brodzik, Dawn Conway, Siri Jodha S. Khalsa, Elena Lobl, James Maslanik, Julianne Stroeve, and Vince Troisi. 2003. Research applications and opportunities using Advanced Microwave Scanning Radiometer-Earth observing system (AMSR-E) data. In: *Proceedings of SPIE*, volume 4894, pages 434–445. SPIE.

- [31] Y. Menard and M. Reynolds. 1991. The Design of the ESA Multiband Imaging Microwave Radiometer MIMR. In: IEEE Geoscience and Remote Sensing Symposium, 1991 (IGARSS'91), volume 4, pages 2359–2363. June 3–6, 1991.
- [32] Sari J. Metsämäki, Saku T. Anttila, Markus J. Huttunen, and Jenni M. Vepsäläinen. 2005. A feasible method for fractional snow cover mapping in boreal zone based on a reflectance model. *Remote Sensing of Environment* 95, pages 77–95.
- [33] James R. Miller, John E. Geysler, Alfred T. C. Chang, and Thomas T. Wilheit. 1982. Observations of Oceanic Surface-wind Fields from Nimbus-7 Microwave Radiometer. *IEEE Transactions on Geoscience and Remote Sensing* GE-20, no. 4, pages 550–554.
- [34] HEG – HDF to GeoTIFF Conversion Tool home page. <http://newsroom.gsfc.nasa.gov/sdptoolkit/HEG/HEGHome.html>. (accessed: May 20th, 2010).
- [35] National Oceanic and Atmospheric Administration. 2006. NOAA KLM User's Guide. URL <http://www.ncdc.noaa.gov/oa/pod-guide/ncdc/docs/klm/index.htm>. (accessed: May 20th, 2010).
- [36] Eni G. Njoku, J. M. Stacey, and Frank T. Barath. 1980. The Seasat Scanning Multichannel Microwave Radiometer (SMMR): Instrument Description and Performance. *IEEE Journal of Oceanic Engineering* OE-5, no. 2, pages 100–115.
- [37] National Board of Waters. 1984. Hydrologiset havainto- ja mittausmenetelmät. Number 47 in Publications of the National Board of Waters. Helsinki, Finland. ISBN 951-46-7491-X, 88 pages. In Finnish.
- [38] Chris Oliver and Shaun Quegan. 1998. Understanding Synthetic Aperture Radar Images. Artech House, Boston, London. ISBN 0-890-06850-X, 512 pages.

- [39] Prem C. Pandey and Ramesh K. Kakar. 1982. An empirical microwave emissivity model for a foam-covered sea. *IEEE Journal of Oceanic Engineering* OE-7, no. 3, pages 135–140.
- [40] M. Pardé, Kalifa Goïta, and Alain Royer. 2007. Inversion of a passive microwave snow emission model for water equivalent estimation using airborne and satellite data. *Remote Sensing of Environment* 111, no. 2-3, pages 346–356. *Remote Sensing of the Cryosphere Special Issue*.
- [41] Oleg Pokrovsky and Jean-Louis Roujean. 2002. Land surface albedo retrieval via kernel-based BRDF modeling: I. Statistical inversion method and model comparison. *Remote Sensing of Environment* 84, no. 1, pages 100–119.
- [42] Jouni Pulliainen. 2004. Kaukokartoitushavaintojen mallinnus- ja tulkin-tamenetelmät. TKK, Avaruustekniikan laboratorio. In Finnish.
- [43] Jouni Pulliainen. 2006. Mapping of snow water equivalent and snow depth in boreal and sub-arctic zones by assimilating space-borne microwave radiometer data and ground-based observations. *Remote Sensing of Environment* 101, no. 2, pages 257–269.
- [44] Jouni Pulliainen, Marcus Engdahl, and Martti Hallikainen. 2003. Feasibility of multi-temporal interferometric SAR data for stand-level estimation of boreal forest stem volume. *Remote Sensing of Environment* 85, no. 4, pages 397–409.
- [45] Jouni Pulliainen, Jenni Vepsäläinen, Seppo Kaitala, Martti Hallikainen, Kari Kallio, Vivi Fleming, and Petri Maunula. 2004. Regional water quality map-ping through the assimilation of spaceborne remote sensing data to ship-based transect observations. *Journal of Geophysical Research* 109. C12009.
- [46] Jouni T. Pulliainen, Jochen Grandell, and Martti T. Hallikainen. 1999. HUT Snow Emission Model and its Applicability to Snow Water Equivalent Re-trieval. *IEEE Transactions on Geoscience and Remote Sensing* 37, no. 3, pages 1378–1390.

- [47] Jouni T. Pulliainen, Kari Heiska, Juha Hyyppä, and Martti T. Hallikainen. 1994. Backscattering Properties of Boreal Forests at the C- and X-Bands. *IEEE Transactions on Geoscience and Remote Sensing* 32, no. 5, pages 1041–1050.
- [48] Jouni T. Pulliainen, Lauri Kurvonen, and Martti T. Hallikainen. 1999. Multi-temporal behavior of L- and C-band SAR observations of boreal forests. *IEEE Transactions on Geoscience and Remote Sensing* 37, no. 2, pages 927–937.
- [49] RADARSAT International. 2000. RADARSAT Data Products Specifications. RSI-GS-026, Revision 3/0.
- [50] K. S. Rao, S. Raju, and J. R. Wang. 1993. Estimation of Soil Moisture and Surface Roughness Parameters from Backscattering Coefficient. *IEEE Transactions on Geoscience and Remote Sensing* 31, no. 5, pages 1094–1099.
- [51] Sirpa Rasmus. 2005. Snow pack structure characteristics in Finland - measurements and modelling. Ph.D. thesis, University of Helsinki, Finland. Report series in Geophysics, No 48.
- [52] W. Gareth Rees. 2005. Remote sensing of snow and ice. CRC Press. ISBN 0-415-29831-8, 285 pages.
- [53] Marja Reuna, Jaakko Perälä, and Seppo Aitamurto. 1993. Lumen aluevesiarvoja Suomessa vuosina 1946–1993. Areal snow water equivalent values in Finland in the years 1946–1993. Number 165 in Publications of Water and Environment Administration – series A. Helsinki, Finland. ISBN 951-47-8447-2, 284 pages. In Finnish.
- [54] E. Salonen, S. Karhu, P. Jokela, W. Zhang, S. Uppala, H. Aulamo, and S. Sarkkula. 1990. Study of propagation phenomena for low availabilities. ESA Contract report 8025/88/NL/PR, Helsinki University of Technology, Espoo, Finland.

- [55] Laurie J. Schmidt. 2000. NASA Earth Observatory: The Universal Language of HDF-EOS. <http://earthobservatory.nasa.gov/Features/HDFEOS/>. (accessed: May 20th, 2010).
- [56] C. T. Swift, L. S. Fedor, and R. O. Ramseier. 1985. An algorithm to measure sea ice concentration with microwave radiometers. *Journal of Geophysical Research* 90, no. C1, pages 1087–1099.
- [57] Matias Takala. 2009. Snow water equivalent (SN-OBS-4) algorithm for non-mountainous areas. Presentation in HydroSAF Snow training workshop, November 27th, 2009. Helsinki, Finland.
- [58] Albert Tarantola and Bernard Valette. 1982. Generalized Nonlinear Inverse Problems Solved Using the Least Squares Criterion. *Reviews of Geophysics and Space Physics* 20, no. 2, pages 219–232.
- [59] Albert Tarantola and Bernard Valette. 1982. Inverse Problems = Quest for Information. *Journal of Geophysics* 50, pages 159–170.
- [60] Fawwatz T. Ulaby, Richard K. Moore, and Adrian K. Fung. 1981. *Microwave Remote Sensing: Active and Passive, volume I, Microwave Remote Sensing Fundamentals and Radiometry*. Addison-Wesley Publishing Company. ISBN 0-201-10759-7, 456 pages.
- [61] Pam Vass and Bruce Battrick (editors). 1992. *ERS-1 Product Specification*. European Space Agency, The Netherlands. ISBN 92-9092-033-5. ESA-SP-1149.
- [62] Bertel Vehviläinen. 1994. The watershed simulation and forecasting system in the National Board of Waters and Environment. Number 17 in Publications of the National Board of Waters and the Environment. Helsinki, Finland.
- [63] Bertel Vehviläinen, Markus Huttunen, and Inese Huttunen. 2005. Hydrological forecasting and real time monitoring in Finland: The watershed simulation

and forecasting system (WSFS). In: *Innovation, Advances and Implementation of Flood Forecasting Technology*. Tromsø, Norway.

- [64] Robert J. Vos, Paul G. J. ten Brummelhuis, and Herman Gerritsen. 2000. Integrated data-modelling approach for suspended sediment transport on a regional scale. *Coastal Engineering* 41, no. 1-3, pages 177–200.
- [65] Stephen G. Warren. 1982. Optical properties of snow. *Reviews of Geophysics and Space Physics* 20, no. 1, pages 67–89.
- [66] Thomas T. Wilheit, James R. Greaves, James A. Gatlin, Daesoo Han, Brian M. Krupp, Andrew S. Milman, and Edward S. Chang. 1984. Retrieval of Ocean Surface Parameters from the Scanning Multifrequency Microwave Radiometer (SMMR) on the Nimbus-7 Satellite. *IEEE Transactions on Geoscience and Remote Sensing* GE-22, no. 2, pages 133–143.
- [67] L.L. Wilson, Leung Tsang, Jenq-Neng Hwang, and Chi-Te Chen. 1999. Mapping snow water equivalent by combining a spatially distributed snow hydrology model with passive microwave remote-sensing data. *IEEE Transactions on Geoscience and Remote Sensing* 37, no. 2, pages 690–704.

Errata

Errata of [P II]

Page 3, last row: The first T_{37H} should be T_{37V} .

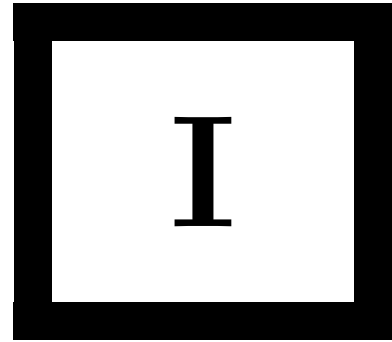
Errata of [P III]

The flow chart in Figure 5: the iteration condition should read $d < min$ instead of $d > min$.

Errata of [P V]

Equation (10) in page 5 should read

$$var(\hat{x}) = \frac{\sum_{i=1}^n \left(\frac{1}{\sigma_i} b_{i1} \right)^2 + \frac{1}{\sigma_{REF}^2}}{\left(\sum_{i=1}^n \frac{1}{\sigma_i^2} b_{i1}^2 + \frac{1}{\sigma_{REF}^2} \right)^2}$$



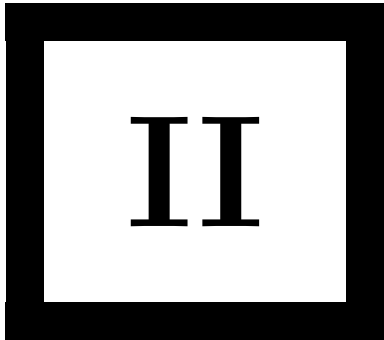
Publication I

J. Pulliainen, J-P. Kärnä, and M. Hallikainen. 1993. Development of geophysical retrieval algorithms for the MIMR. *IEEE Transactions on Geoscience and Remote Sensing* 31, no. 1, pages 268–277.

© 1993 IEEE.

Reprinted with permission.

This material is posted here with permission of the IEEE. Such permission of the IEEE does not in any way imply IEEE endorsement of any of Aalto University School 's products or services. Internal or personal use of this material is permitted. However, permission to reprint/republish this material for advertising or promotional purposes or for creating new collective works for resale or redistribution must be obtained from the IEEE by writing to pubs-permissions@ieee.org. By choosing to view this material, you agree to all provisions of the copyright laws protecting it.



II

Publication II

J-P. Kärnä, J. Lemmetyinen, M. Hallikainen, P. Lahtinen, J. Pulliainen, and M. Takala. 2007. Operational snow map production for whole Eurasia using microwave radiometer and ground-based observations. In: Proceedings of the IEEE International Geoscience and Remote Sensing Symposium 2007 (IGARSS'07), pages 1456–1459. Barcelona, Spain. 23–28 July 2007.

© 2007 IEEE.

Reprinted with permission.

This material is posted here with permission of the IEEE. Such permission of the IEEE does not in any way imply IEEE endorsement of any of Aalto University School's products or services. Internal or personal use of this material is permitted. However, permission to reprint/republish this material for advertising or promotional purposes or for creating new collective works for resale or redistribution must be obtained from the IEEE by writing to pubs-permissions@ieee.org. By choosing to view this material, you agree to all provisions of the copyright laws protecting it.

Publication III

J-P. Kärnä, J. Pulliainen, K. Luojus, N. Patrikainen, M. Hallikainen, S. Metsämäki, and M. Huttunen. 2004. Mapping of snow covered area using combined SAR and optical data. In: Proceedings of the 4th International Symposium on Retrieval of Bio- and Geophysical Parameters from SAR Data for Land Applications. Innsbruck, Austria. 16–19 November 2004.

© 2004 Authors



IV

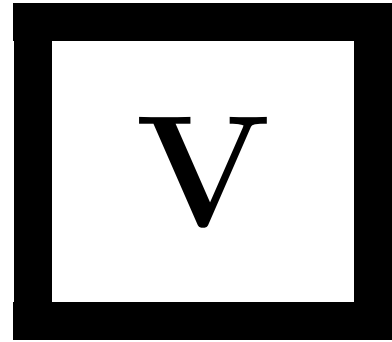
Publication IV

J-P. Kärnä, J. Pulliainen, M. Huttunen, and J. Koskinen. 2002. Assimilation of SAR data to operational hydrological runoff and snow melt forecasting model. In: Proceedings of the IEEE International Geoscience and Remote Sensing Symposium 2002 (IGARSS'02), volume 2, pages 1146–1148. Toronto, Canada. 24–28 June 2002.

© 2002 IEEE.

Reprinted with permission.

This material is posted here with permission of the IEEE. Such permission of the IEEE does not in any way imply IEEE endorsement of any of Aalto University School's products or services. Internal or personal use of this material is permitted. However, permission to reprint/republish this material for advertising or promotional purposes or for creating new collective works for resale or redistribution must be obtained from the IEEE by writing to pubs-permissions@ieee.org. By choosing to view this material, you agree to all provisions of the copyright laws protecting it.



Publication V

J-P Kärnä and J. Pulliainen. 2007. A statistical inversion tool for retrieving geophysical parameters from remote sensing data. Report 68, Laboratory of Space Technology, Helsinki University of Technology, Espoo, Finland. ISBN 978-951-22-8636-2, 30 pages.

© 2007 J-P Kärnä and J. Pulliainen